SYMMETRY AND AUTOMATED BRANCH FOLLOWING FOR A SEMILINEAR ELLIPTIC PDE ON A FRACTAL REGION

JOHN M. NEUBERGER, NÁNDOR SIEBEN, AND JAMES W. SWIFT

Abstract. We apply the Gradient-Newton-Galerkin-Algorithm (GNGA) of Neuberger & Swift to find solutions to a semilinear elliptic Dirichlet problem on the region whose boundary is the Koch snowflake. In a recent paper, we described an accurate and efficient method for generating a basis of eigenfunctions of the Laplacian on this region. In that work, we used the symmetry of the snowflake region to analyze and post-process the basis, rendering it suitable for input to the GNGA. The GNGA uses Newton's method on the eigenfunction expansion coefficients to find solutions to the semilinear problem. This article introduces the *bifurcation digraph*, an extension of the lattice of isotropy subgroups. For our example, the bifurcation digraph shows the 23 possible symmetry types of solutions to the PDE and the 59 generic symmetry-breaking bifurcations among these symmetry types. Our numerical code uses continuation methods, and follows branches created at symmetry-breaking bifurcations, so the human user does not need to supply initial guesses for Newton's method. Starting from the known trivial solution, the code automatically finds at least one solution with each of the symmetry types that we predict can exist. Such computationally intensive investigations necessitated the writing of automated branch following code, whereby symmetry information was used to reduce the number of computations per GNGA execution and to make intelligent branch following decisions at bifurcation points.

1. Introduction.

We seek numerical solutions to the semilinear elliptic boundary value problem

$$\begin{aligned} \Delta u + f_\lambda(u) &= 0 \text{ in } \Omega \\ u &= 0 \text{ on } \partial\Omega, \end{aligned} \tag{1}$$

where Δ is the Laplacian operator, $\Omega \subset \mathbb{R}^2$ is the region whose boundary $\partial\Omega$ is the Koch snowflake, $u : \Omega \to \mathbb{R}$ is the unknown function, and $f_\lambda : \mathbb{R} \to \mathbb{R}$ is a one-parameter family of odd functions. For convenience, we refer to Ω as the *Koch snowflake region*. This article is one of the first to consider a nonlinear PDE on a region with fractal boundary. In this paper, we choose the nonlinearity to be

$$f_\lambda(u) = \lambda u + u^3, \tag{2}$$

and treat $\lambda \in \mathbb{R}$ as the bifurcation parameter. When the parameter is fixed, we will sometimes use f in place of f_λ. Using this convention, note that $\lambda = f'(0)$.

This paper exploits the hexagonal symmetry of the Koch snowflake region, and the fact that f is odd. Our nonlinear code would work with any region with hexagonal symmetry and any odd 'superlinear' function f (see [2]), and with minor modification for other classes of nonlinearities as well. We chose to work with odd f primarily because of the rich symmetry structure. The explicit shape of Ω represents a considerable technological challenge for the computation of the eigenfunctions [11, 20], which are required as input to the nonlinear code.

It is well known that the eigenvalues of the Laplacian under this boundary condition satisfy

$$0 < \lambda_1 < \lambda_2 \leq \lambda_3 \leq \cdots \to \infty, \tag{3}$$

2000 *Mathematics Subject Classification.* 20C35, 35P10, 65N25.
Key words and phrases. Snowflake, Symmetry, Bifurcation, Semilinear Elliptic PDE, GNGA.
Partially supported by NSF Grant DMS-0074326.
September 16, 2005.

and that the corresponding eigenfunctions

$$\{\psi_j\}_{j\in\mathbb{N}} \tag{4}$$

are an orthogonal basis of both the Sobolev space $H = H_0^{1,2}(\Omega)$ and the larger Hilbert space $L^2 = L^2(\Omega)$, with the inner products

$$\langle u, v\rangle_H = \int_\Omega \nabla u \cdot \nabla v \, dx \quad \text{and} \quad \langle u, v\rangle_2 = \int_\Omega u \, v \, dx,$$

respectively. Using the Gradient-Newton-Galerkin-Algorithm (GNGA, see [19]) we seek approximate solutions $u = \sum_{j=1}^{M} a_j\psi_j$ to (1) by applying Newton's method to the eigenfunction expansion coefficients of the gradient $\nabla J(u)$ of a nonlinear functional J whose critical points are the desired solutions. The definition of J, the required variational equations, a description of the GNGA, and a brief history of the problem are the subject of Section 2.

The GNGA requires as input a basis spanning a sufficiently large but finite dimensional subspace $B_M = \text{span}\{\psi_1, \ldots, \psi_M\}$, corresponding to the first M eigenvalues $\{\lambda_j\}_{j=1}^{M}$. As described in [20], a grid G_N of N carefully placed points is used to approximate the eigenfunctions. These are the same grid points used for the numerical integrations required by Newton's method. Section 3 briefly describes the process we use for generating the eigenfunctions.

Section 4 concerns the effects of symmetry on automated branch following. The symmetry theory for linear operators found in [20] is summarized and then the extensions required for nonlinear operators are described. Symmetry-breaking bifurcations are analyzed in a way that allows an automated system to follow the branches created at the bifurcations. As we develop the theory, we present specific examples applying the general theory to equation (1) on the snowflake region. In particular, we find that there are 23 different symmetry types of solutions to (1), and 59 generic symmetry-breaking bifurcations. The symmetry types and bifurcations among them are summarized in a *bifurcation digraph*, which generalizes the well-known lattice of isotropy subgroups (see [6]). The introduction of the bifurcation digraph is a central accomplishment of this paper.

Section 5 describes how understanding the symmetry allows remarkable increases in the efficiency of the GNGA. Section 6 describes the automated branch following. We use repeated executions of the GNGA or a slightly modified algorithm (parameter-modified GNGA) to follow solution branches of (1, 2). The GNGA uses Newton's method, which is known to work well if it has a good initial approximation. The main shortcoming of Newton's method is that is works poorly without a good initial approximation. We avoid this problem by starting with the trivial solution ($u = 0$). The symmetry-breaking bifurcations of the trivial solution are found by the algorithm and the primary branches are started. The program then recursively follows the the branches by continuation methods, and then follows the new branches created at symmetry-breaking bifurcations. To follow an existing branch, we vary λ slightly between executions. To start new solution branches created at bifurcation points, we treat λ as a variable and fix one of the null eigenfunctions of the Hessian evaluated at the bifurcation point. The symmetry analysis tells which null eigenfunction to use. In this way solutions with all 23 symmetry types are found automatically, starting from $u = 0$, without having to guess any approximations for Newton's method.

In our experiments, many bifurcation diagrams were generated by applying the techniques mentioned above. A selection of these diagrams are provided in Section 7, along with contour plots of solutions to (1) corresponding to each of the 23 symmetry types predicted to exist. We include evidence of the convergence of our algorithm as the number of modes M and grid points N increase.

Many extensions to our work are possible, including enforcing different boundary conditions on the same region, solving similar semilinear equations on other fractal regions, and applying the methodology to partial difference equations (PdE) on graphs [18]. Section 8 discusses some of these possible extensions. In particular, we are in the process of re-writing the suite of programs. We plan to be able to solve larger problems using a parallel environment. We will be able to solve

problems with larger symmetry groups by automating the extensive group theoretic calculations. This concluding section also has a discussion of the convergence of the GNGA.

2. GNGA.

We now present the variational machinery for studying (1) and follow with a brief description of the general GNGA. Section 6 contains more details of the implementation of the algorithm for our specific problem. Let $F_\lambda(u) = \int_0^u f_\lambda(s)\,ds$ for all $u \in \mathbb{R}$ define the primitive of f_λ. We then define the action functional $J : \mathbb{R} \times H \to \mathbb{R}$ by

$$J(\lambda, u) = \int_\Omega \left\{ \tfrac{1}{2}|\nabla u|^2 - F_\lambda(u) \right\} dx. \tag{5}$$

We will sometimes use $J : H \to \mathbb{R}$ to denote $J(\lambda, \cdot)$. The class of nonlinearities f found (for example) in [2, 3, 18] imply that J is well defined and of class C^2 on H. The choice (2) we make in this paper belongs to that class. It is well known that critical points of J are in fact solutions to (1) (see for example [22]), and vice versa. The choice of H for the domain is crucial to the analysis of the PDE (see [2, 17], and references therein), as well as for understanding the theoretical basis of effective steepest descent algorithms (see [4, 15, 16], for example). We will work in the subspace $B_M = \text{span}\{\psi_1, \ldots, \psi_M\}$, where the twice continuously differentiable eigenfunctions $\{\psi_j\}$ (4) are normalized in L^2, and in the corresponding coefficient space, where $u \in B_M$ if and only if $u = \sum_{j=1}^M a_j\psi_j$ for some coefficient vector $a \in \mathbb{R}^M$. Using the corresponding eigenvalues (3) and integrating by parts, the quantities of interest are

$$g_j = J'(u)(\psi_j) = \int_\Omega \{\nabla u \cdot \nabla\psi_j - f(u)\,\psi_j\} = a_j\lambda_j - \int_\Omega f(u)\,\psi_j \tag{6}$$

and

$$h_{jk} = J''(u)(\psi_j, \psi_k) = \int_\Omega \{\nabla\psi_j \cdot \nabla\psi_k - f'(u)\,\psi_j\,\psi_k\} = \lambda_j\delta_{jk} - \int_\Omega f'(u)\,\psi_j\,\psi_k, \tag{7}$$

where δ_{jk} is the Kronecker delta function. Note that there is no need for numerical differentiation when forming gradient and Hessian coefficient vectors and matrices in implementing Algorithm 2.1; this information is encoded in the eigenfunctions.

The vector $g \in \mathbb{R}^M$ and the $M \times M$ matrix h represent suitable projections of the L^2 gradient and Hessian of J, restricted to the subspace B_M, where all such quantities are defined. For example, for $u = \sum_{j=1}^M a_j\psi_j$, $v = \sum_{j=1}^M b_j\psi_j$, and $w = \sum_{j=1}^M c_j\psi_j$, we have:

$$P_{B_M}\nabla_2 J(u) = \sum_{j=1}^M g_j\psi_j, \;\; J'(u)(v) = g \cdot b, \text{ and } J''(u)(v, w) = hb \cdot c = b \cdot hc.$$

We can identify g with the approximation $P_{B_M}\nabla_2 J(u)$ of $\nabla_2 J(u) = \Delta u + f(u)$, which is defined for $u \in B_M$. The solution χ to the M-dimensional linear system $h\chi = g$ is then identified with the (suitably projected) search direction $(D_2^2 J(u))^{-1}\nabla_2 J(u)$, which is not only defined for $u \in B_M$, but is there equal to $(D_H^2 J(u))^{-1}\nabla_H J(u)$. We use the least squares solution of $h\chi = g$. In practice, the algorithm works even near bifurcation points where the Hessian is not invertible.

The heart of our code is Newton's method in the space of eigenfunction coefficients:

Algorithm 2.1. (GNGA)

(1) Choose initial coefficients $a = \{a_j\}_{j=1}^M$, and set $u = \sum a_j\psi_j$.
(2) Loop
  (a) Calculate the gradient vector $g = \{J'(u)(\psi_j)\}_{j=1}^M$ from equation (6).
  (b) Calculate the Hessian matrix $h = \{J''(u)(\psi_j, \psi_k)\}_{j,\,k=1}^M$ from equation (7).
  (c) Exit loop if $||g||$ is sufficiently small.
  (d) Solve $h\chi = g$ for the Newton search direction $\chi \in \mathbb{R}^M$.
  (e) Replace $a \leftarrow a - \chi$ and update $u = \sum a_j\psi_j$.

(3) Calculate $\mathrm{sig}(h)$ and J for the approximate solution.

If Newton's method converges then we expect that u approximates a solution to the PDE (1), provided M is sufficiently large and the eigenfunctions and numerical integrations are sufficiently accurate. See Section 8.

Our estimate for the Morse index (MI) of the critical point of J is the signature of h, denoted $\mathrm{sig}(h)$, which is defined as the number of negative eigenvalues of h. This measures the number of linearly independent directions away from u in which J decreases quadratically.

The basic Algorithm 2.1 is modified to take advantage of the symmetry of our problem. The M integrations required in step (a) and the $M(M+1)/2$ integrations in step (b) are reduced to smaller numbers if the initial guess has nontrivial symmetry.

We often use a "parameter-modified" version of the GNGA (pmGNGA). In this modification, λ is treated as an unknown variable and one of the M coefficients a_k is fixed. Along a given branch, symmetry generally forces many coefficients to be zero. When a bifurcation point is located by observing a change in MI, we can predict the symmetry of the bifurcating branches using the symmetry of the null eigenfunctions of the Hessian. By forcing a small nonzero component in the direction of a null eigenfunction (orthogonal to the old branch's smaller invariant subspace), we can assure that the pmGNGA will not converge to a solution lying on the old branch. Another benefit of the pmGNGA is that it can handle a curve bifurcating to the right as well as one bifurcating to the left. In our system, the branches that bifurcate to the right have saddle node bifurcations where they turn around and go to the left. The pmGNGA can follow such branches while the normal GNGA cannot.

The implementation of pmGNGA is not difficult. The M equations are still

$$g_i = J'(u)(\psi_i) = 0,$$

but the M unknowns are

$$\tilde{a} = (a_1, \ldots, a_{k-1}, \lambda, a_{k+1}, \ldots, a_M),$$

and the value of one coefficient, a_k, is fixed. Consequently, we replace the Hessian matrix h with a new matrix $\tilde{h}$ where the k-th column is set to $\partial g_i/\partial\lambda = -a_i$:

$$\tilde{h}_{ij} = \begin{cases} h_{ij} & \text{if } j \neq k \\ -a_i & \text{if } j = k \end{cases}.$$

The search direction $\tilde{\chi}$ is the solution to the system $\tilde{h}\tilde{\chi} = g$. The pmGNGA step is

$$\tilde{a} \leftarrow \tilde{a} - \tilde{\chi},$$

and then u and λ are updated. After Newton's method converges, the k-th column of the original h_{ij} is calculated and the MI of the solution, $\mathrm{sig}(h)$, is computed.

We conclude this section with a very brief history of the analytical and numerical aspects of the research into (1) given our type of nonlinearity f. Our introduction to this general subject was [2], where a sign-changing existence result was proven. This theorem is extended in [3]; we indicate briefly in Section 7 where this so-called CCN solution can be found on our bifurcation diagrams. The GNGA was developed in [19], wherein a much more detailed description of the variational structure and numerical implementation can be found. The computational efforts related to this current project are somewhat more sophisticated. The more important aspects of our improvements are explained in Sections 4 and 6. This article is the second of our published works concerning GNGA for general regions; see [8] where the region is a Bunimovich stadium. The article [4] was our first success in using symmetry to find higher MI solutions. The details concerning the grid, basis generation, and subsequent symmetry analysis for the snowflake are in [20]. The article [17] provides a historical overview of the authors' experimental results using variants of the Mountain Pass Algorithm (MPA, MMPA, HLA) and the GNGA, as well as recent analytical results and a list of open problems; the references found therein are extensive.

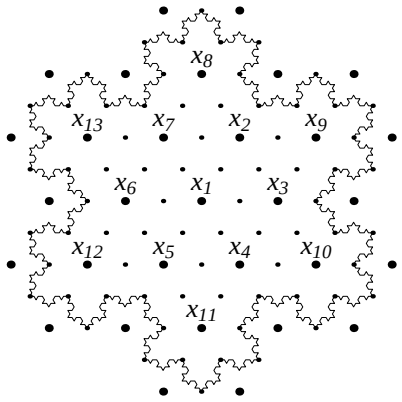

FIGURE 1. The Koch snowflake $\partial\Omega$ with $N = 13$ labelled grid points $\{x_i\}_{i=1}^{13}$ at level $\ell = 2$. At this level, the grid used by [11] consists of the $N_{\mathrm{LNR}}(2) = 37$ large and small points inside the snowflake, along with 48 small points on $\partial\Omega$. The points outside of the snowflake are ghost points we use to enforce the boundary conditions; these ghost points are not used by our nonlinear code.

ℓ	1	2	3	4	5	6
N	1	13	133	1261	11605	105469

TABLE 1. The number N of interior grid points as a function of the level ℓ. The spacing between grid points is $h = h_{\mathrm{NSS}}(\ell) = 2/3^{\ell}$. We typically use level $\ell = 5$ in our nonlinear experiments.

3. The Basis of Eigenfunctions.

In [20], we describe theoretical and computational results that lead to the generation of a basis of eigenfunctions solving

$$\Delta u + \lambda u = 0 \text{ in } \Omega, \quad u = 0 \text{ on } \partial\Omega. \tag{8}$$

That paper details the grid technique and symmetry analysis that accompanied the effort; we briefly summarize those results in this section.

The Koch snowflake is a well known fractal, with Hausdorff dimension $\log_3 4$. Following Lapidus, Neuberger, Renka, and Griffith [11], we take our snowflake to be inscribed in a circle of radius $\frac{\sqrt{3}}{3}$ centered about the origin. With this choice, the polygonal approximations used in the fractal construction have side length that are powers of $1/3$. We use a triangular grid G_N of N points to approximate the snowflake region. Then, we identify $u : G_N \to \mathbb{R}$ with $u \in \mathbb{R}^N$, that is,

$$u(x_i) = u_i \tag{9}$$

at grid points $x_i \in G_N$. Figure 1 depicts a low level grid used in [20] to compute eigenfunctions; we use this same grid for our nonlinear experiments. The number of grid points on other levels are in Table 1.

Our method of imposing the zero-Dirichlet boundary conditions can be summarized as

$$\begin{aligned} -\Delta u(x) \approx \frac{2}{3h^2}((12 - \text{number of interior neighbors})u(x) - \\ \sum\{\text{interior neighbor values of } u\}). \end{aligned} \tag{10}$$

Using the differencing scheme in (10) and the grid depicted in Figure 1, we computed [20] eigenvalues and eigenfunctions for (8) using ARPACK. Table 2 lists approximations of the first

k	1	2	3	4	5	6	7	8	9	10
λ_k	39.4	97.4	97.4	165.4	165.4	190.4	208.6	272.4	272.4	312.4

TABLE 2. Approximate values for the first ten eigenvalues to the Dirichlet problem. For more values with greater precision see [20].

ten eigenvalues; these values are primary bifurcation points. The ARPACK is based upon an algorithmic variant of the Arnoldi process called the Implicitly Restarted Arnoldi Method (see [12]) and is ideally suited for finding the eigen-pairs of the large sparse matrices associated with the discretization of the Laplacian.

4. Symmetry: The Lattice of Isotropy Subgroups and The Bifurcation Digraph.

This section describes equivariant bifurcation theory (see, for example [6] or [7]) as it applies to the branching of solutions to equation (1). We are able to describe the expected symmetry types of solutions to (1), as traditionally arranged in a lattice of isotropy subgroups. We introduce the *bifurcation digraph*, essentially a refinement of the lattice, which shows every possible generic bifurcation from one symmetry type to another as a directed edge which is labelled with information about the bifurcation. This digraph is of interest in its own right and summarizes the essential information required by our automated branch following code. In this project, GAP (Groups, Algorithms, and Programming, see [5]) was used to verify our symmetry analysis; in our continuing projects GAP is a necessary tool when the symmetry calculations are too complicated to be done by hand. Matthews [14] has used GAP to do similar calculations. We apply this methodology to the snowflake domain being considered in this paper. The analysis shows that solutions fall into 23 symmetry types, and that there are 59 types of generic symmetry breaking bifurcations.

Group Actions and the Lattice of Isotropy Subgroups. Let Γ be a compact Lie group and V be a real vector space. A *representation* of Γ is a homomorphism $\alpha : \Gamma \to GL(V)$. Where convenient, we identify $GL(V)$ with the set of invertible matrices with real coefficients. Every representation α corresponds to a unique *group action* of Γ on V by the rule $\gamma \cdot v := \alpha(\gamma)(v)$ for all $\gamma \in \Gamma$ and $v \in V$. We will usually use the action rather than the representation. The *group orbit* of v is $\Gamma \cdot v = \{\gamma \cdot v \mid \gamma \in \Gamma\}$.

Example 4.1. The standard action of the dihedral group

$$\mathbb{D}_6 := \langle \rho, \sigma \mid \rho^6 = \sigma^2 = 1, \rho\sigma = \sigma\rho^5 \rangle$$

on the plane is

$$\begin{aligned} \rho \cdot (x, y) &= \left(\tfrac{1}{2}x + \tfrac{\sqrt{3}}{2}y, -\tfrac{\sqrt{3}}{2}x + \tfrac{1}{2}y\right) \\ \sigma \cdot (x, y) &= (-x, y) \\ \tau \cdot (x, y) &= (x, -y). \end{aligned} \tag{11}$$

In this action ρ is a rotation by 60°, σ is a reflection across the y-axis, and τ is a reflection across the x-axis. While the group is generated by ρ and σ, we have defined $\tau = \rho^3\sigma$ since the reflection across the x-axis is so important. Note that $\sigma\tau = \tau\sigma = \rho^3$. We will denote subgroups of $\mathbb{D}_6$ by listing the generators. For example $\langle \rho^2, \tau \rangle = \{1, \rho^2, \rho^4, \tau, \rho^2\tau, \rho^4\tau\} \cong \mathbb{D}_3$.

The symmetry group of the Koch Snowflake region Ω is $\mathbb{D}_6$. The standard $\mathbb{D}_6$ group action of (11) is not the only action we consider. For a function $u \in L^2(\Omega)$ and group element $\gamma \in \mathbb{D}_6$, we define $(\gamma \cdot u)(x) = u(\gamma^{-1} \cdot x)$. In this paper, the vectors $u_i = u(x_i)$, for a given grid $G_N = \{x_i\}_{i=1}^N$, are discrete approximations of functions on Ω. The $\mathbb{D}_6$ group action on $u_i \in \mathbb{R}^N$ is a permutation of the components: $(\gamma \cdot u)_i = u(\gamma^{-1} \cdot x_i)$. Given a function $u \in L^2(\Omega)$ or $\mathbb{R}^N$, the group orbit $\mathbb{D}_6 \cdot u$ consists of functions obtained from u by a reflection or rotation.

Example 4.2. The group $\mathbb{D}_6 \times \mathbb{Z}_2$, where $\mathbb{Z}_2 = \{1, -1\}$, acts on $L^2(\Omega)$ in a natural way. For all $(\gamma, z) \in \mathbb{D}_6 \times \mathbb{Z}_2$, define

$$(\gamma, z) \cdot u = z(\gamma \cdot u).$$

We will denote $(\gamma, 1) \in \mathbb{D}_6 \times \mathbb{Z}_2$ by γ and $(\gamma, -1) \in \mathbb{D}_6 \times \mathbb{Z}_2$ by $-\gamma$. With this natural notation $(-\gamma) \cdot u = -(\gamma \cdot u)$, which we call simply $-\gamma \cdot u$.

Let us recall some facts about group actions, following [6]. The *isotropy subgroup* or *stabilizer of* $v \in V$ *in* Γ is

$$\mathrm{Stab}(v, \Gamma) := \{\gamma \in \Gamma \mid \gamma \cdot v = v\}.$$

Other notations for $\mathrm{Stab}(v, \Gamma)$ are Γ_v. The isotropy subgroup of v is often called the little group of v. The Γ is necessary when several groups act on the same space. If the group is understood, we may simply write $\mathrm{Stab}(v)$ in place of $\mathrm{Stab}(v, \Gamma)$. The isotropy subgroup measures how much symmetry v has. The *stabilizer of a subset* $W \subseteq V$ *in* Γ is then defined as $\mathrm{Stab}(W, \Gamma) := \{\gamma \in \Gamma \mid \gamma \cdot W = W\}$. This must be distinguished from the *point stabilizer of a subset*

$$\mathrm{pStab}(W, \Gamma) := \{\gamma \in \Gamma \mid \gamma \cdot v = v \text{ for all } v \in W\} = \bigcap \{\mathrm{Stab}(v, \Gamma) \mid v \in W\}.$$

Another commonly used notation is Γ_W for the stabilizer and $\Gamma_{(W)}$ for the point stabilizer. Note that $\mathrm{pStab}(W, \Gamma)$ is always normal in $\mathrm{Stab}(W, \Gamma)$, and the *effective symmetry group acting on* W is $\mathrm{Stab}(W, \Gamma)/\mathrm{pStab}(W, \Gamma)$, which acts faithfully on W.

If Σ is a subgroup of Γ then the *fixed point subspace of* Σ *in* V is

$$\mathrm{Fix}(\Sigma, V) := \{v \in V \mid \ \gamma \cdot v = v \text{ for all } \gamma \in \Sigma\}.$$

Another notation for the fixed point subspace is V_Σ. Often, we will drop the V when the space on which Γ acts is clear.

An *isotropy subgroup* of the Γ action on V is the stabilizer of some point $v \in V$. For some group actions, not every subgroup of Γ is an isotropy subgroup. A necessary and sufficient condition for Σ to be an isotropy subgroup of a Γ action on V is that $\Sigma = \mathrm{pStab}(\mathrm{Fix}(\Sigma, V), \Gamma)$, that is

$$\Sigma \text{ is an isotropy subgroup} \iff \Sigma = \mathrm{pStab}(\mathrm{Fix}(\Sigma)). \tag{12}$$

Example 4.3. Consider the $\mathbb{D}_6$ action on the plane $\mathbb{R}^2$ described in Example 4.1. Then $\mathrm{Stab}((0,1), \mathbb{D}_6) = \{1, \sigma\}$, $\mathrm{Stab}(\Omega, \mathbb{D}_6) = \mathbb{D}_6$, and $\mathrm{pStab}(\Omega, \mathbb{D}_6) = \{1\}$. The subgroup $\langle\rho\rangle$ is not an isotropy subgroup of this group action because $\mathrm{Fix}(\langle\rho\rangle, \mathbb{R}^2) = \{(0,0)\}$, but $\mathrm{pStab}((0,0), \mathbb{D}_6) = \mathbb{D}_6$. Thus, there is no point in the plane whose isotropy subgroup is $\langle\rho\rangle$.

Now consider the $\mathbb{D}_6$ action on the function space $L^2(\Omega)$. Start with a function u^* that is zero everywhere except for a small region, and suppose that the region is distinct from each of its nontrivial images under the $\mathbb{D}_6$ action. Then for any subgroup $\Sigma \leq \mathbb{D}_6$, the *average of the function* u^* *over* Σ, defined as

$$P_\Sigma(u^*) = \frac{1}{|\Sigma|} \sum_{\gamma \in \Sigma} \gamma \cdot u^* \tag{13}$$

has isotropy subgroup Σ. Therefore every subgroup of the $\mathbb{D}_6$ action on $L^2(\Omega)$ is an isotropy subgroup. The average over the group is an example of a Haar operator, and $P_\Sigma : V \to \mathrm{Fix}(\Sigma, V)$ is an orthogonal projection operator [30].

Similarly, every subgroup of $\mathbb{D}_6$ is an isotropy subgroup of the $\mathbb{D}_6$ action on $\mathbb{R}^{133}$, the space of functions on our grid at level $\ell = 3$. This follows from averaging the function that is 1 at a generic lattice point, and 0 elsewhere. (A *generic point* is one whose isotropy subgroup is trivial.) Note that the grid at level $\ell = 2$, shown in Figure 1, does not have a generic lattice point. For the action of $\mathbb{D}_6$ on $\mathbb{R}^{13}$, the space of functions on G_{13}, averaging any function over $\langle\rho\rangle$ gives a function with isotropy subgroup $\mathbb{D}_6$. Hence, $\langle\rho\rangle$ is not an isotropy subgroup of the $\mathbb{D}_6$ action on $\mathbb{R}^{13}$.

While the level 3 grid is the smallest of our grids shown in Table 1 with a generic lattice point, we can get by with fewer points. Start with any generic point $x_1 \in \Omega$. Then $\mathbb{D}_6$ acts on the space of functions on the 12 points $\{\gamma \cdot x_1 \mid \gamma \in \mathbb{D}_6\}$. This $\mathbb{D}_6$ action on $\mathbb{R}^{12}$ has the same structure of

isotropy subgroups as the $\mathbb{D}_6$ action on $L^2(\Omega)$, and is the $\mathbb{D}_6$ action used in our GAP calculations. The corresponding 12-dimensional representation is the well-known *regular representation* of $\mathbb{D}_6$ (see [23, 25, 28]).

The symmetry of functions is described by two related concepts. A function $q : V \to \mathbb{R}$ is Γ-*invariant* if $q(\gamma \cdot v) = q(v)$ for all $\gamma \in \Gamma$ and all $v \in V$. Similarly, an operator $T : V \to V$ is Γ-*equivariant* if $T(\gamma \cdot v) = \gamma \cdot T(v)$ for all $\gamma \in \Gamma$ and all $v \in V$.

Example 4.4. The energy functional J defined in equation (5) is $\mathbb{D}_6 \times \mathbb{Z}_2$-invariant. The nonlinear PDE (1) can be written as $(\Delta + f)(u) = 0$, where $\Delta + f$ is a $\mathbb{D}_6 \times \mathbb{Z}_2$-equivariant operator. (There are subtleties concerning the domain and range of Δ. See [4] for a careful treatment of the function spaces.) In particular, $\Delta + f$ is $\mathbb{D}_6$-equivariant because the snowflake region Ω has $\mathbb{D}_6$ symmetry, and $(\Delta + f)(-u) = -(\Delta + f)(u)$, since f is odd. As a consequence, if u is a solution to (1), then so is every element in its group orbit $(\mathbb{D}_6 \times \mathbb{Z}_2) \cdot u$.

The isotropy subgroups and fixed point subspaces are important because of the following simple yet powerful results. See [6] or [7].

Proposition 4.5. *Suppose* Γ *acts linearly on* V, $T : V \to V$ *is* Γ*-equivariant and* Σ *is an isotropy subgroup of* Γ.

(a) *If* $v \in \mathrm{Fix}(\Sigma)$ *then* $T(v) \in \mathrm{Fix}(\Sigma)$. *Thus,* $T|_{\mathrm{Fix}(\Sigma)} : \mathrm{Fix}(\Sigma) \to \mathrm{Fix}(\Sigma)$ *is defined.*
(b) $\mathrm{Stab}(\mathrm{Fix}(\Sigma)) = N_\Gamma(\Sigma)$, *the normalizer of* Σ *in* Γ.
(c) $T|_{\mathrm{Fix}(\Sigma)}$ *is* $N_\Gamma(\Sigma)$*-equivariant.*
(d) $T|_{\mathrm{Fix}(\Sigma)}$ *is* $N_\Gamma(\Sigma)/\Sigma$*-equivariant, and* $N_\Gamma(\Sigma)/\Sigma$ *acts faithfully on* $\mathrm{Fix}(\Sigma)$.

If Σ is a subgroup of Γ, the normalizer of Σ in Γ is defined to be $N_\Gamma(\Sigma) := \{\gamma \in \Gamma \mid \gamma\Sigma = \Sigma\gamma\}$, which is the largest subgroup of Γ for which Σ is a normal subgroup. The presence of the normalizer in Proposition 4.5(b) is interesting, since the normalizer is a property of the abstract groups, and is independent of the group action.

Example 4.6. As a consequence of Proposition 4.5, we can solve the PDE (1), written as $(\Delta+f)(u) = 0$, by restricting u to functions in $\mathrm{Fix}(\Sigma, L^2(\Omega))$. This leads to a simpler problem since the function space $\mathrm{Fix}(\Sigma, L^2(\Omega))$ is simpler than $L^2(\Omega)$. An example of this is in Costa, Ding, and Neuberger [4]. The techniques of that paper, applied to our problem, would find sign-changing solutions with Morse index 2 within the space $\mathrm{Fix}(\mathbb{D}_6, L^2(\Omega))$. This space consists of all functions which are unchanged under all of the rotations and reflections of the snowflake region.

Proposition (4.5) also applies to the GNGA, since the Newton's method iteration mapping is $\mathbb{D}_6 \times \mathbb{Z}_2$-equivariant. If the initial guess is in a particular fixed point subspace, all the iterates will be in that fixed point subspace. This understanding can be used to speed numerical calculations, as described in Section 5.

Two subgroups Σ_1, Σ_2 of Γ are conjugate ($\Sigma_1 \sim \Sigma_2$) if $\Sigma_1 = \gamma\Sigma_2\gamma^{-1}$ for some $\gamma \in \Gamma$. We define the *symmetry type* of $v \in V$ for the Γ action to be the conjugacy class of $\mathrm{Stab}(v, \Gamma)$. Note that $\mathrm{Stab}(\gamma \cdot v) = \gamma\,\mathrm{Stab}(v)\gamma^{-1}$. Thus, every element of a group orbit $\Gamma \cdot v$ has the same symmetry type.

Example 4.7. The symmetry type of a solution u to our PDE (1) for the $\mathbb{D}_6 \times \mathbb{Z}_2$ action is the conjugacy class of $\mathrm{Stab}(u, \mathbb{D}_6 \times \mathbb{Z}_2)$; we refer to this as the symmetry type of u, without reference to $\mathbb{D}_6 \times \mathbb{Z}_2$. The discussion of $\mathbb{D}_6$ acting on $L^2(\Omega)$ in Example 4.3 can easily be extended to $\mathbb{D}_6 \times \mathbb{Z}_2$ acting on $L^2(\Omega)$. Note that if $-1 \in \Sigma \leq \mathbb{D}_6 \times \mathbb{Z}_2$, then the average of any function over Σ is $u = 0$. Therefore the only isotropy subgroup of $\mathbb{D}_6 \times \mathbb{Z}_2$ which contains -1 is $\mathbb{D}_6 \times \mathbb{Z}_2$ itself. On the other hand, the argument in Example 4.3 shows that any subgroup of $\mathbb{D}_6 \times \mathbb{Z}_2$ which does not contain -1 is an isotropy subgroup. Therefore, $\Sigma \leq \mathbb{D}_6 \times \mathbb{Z}_2$ is an isotropy subgroup of this group action if and only if $\Sigma = \mathbb{D}_6 \times \mathbb{Z}_2$ or $-1 \notin \Sigma$.

This result allowed us to compute the isotropy subgroups by hand. We verified our calculations using GAP and the characterization in Equation (12) for the action of $\mathbb{D}_6 \times \mathbb{Z}_2$ on $\mathbb{R}^{12}$ described in

Example 4.3. There are exactly 23 conjugacy classes of isotropy subgroups for the $\mathbb{D}_6 \times \mathbb{Z}_2$ action on $L^2(\Omega)$. Thus, a solution to the PDE (1) has one of 23 different symmetry types.

Let $\mathcal{S} = \{S_i\}$ denote the set of all symmetry types of a Γ action on V. The set $\mathcal{S}$ has a natural partial order, with $S_i \leq S_j$ if there exits $\Sigma_i \in S_i$ and $\Sigma_j \in S_j$ such that $\Sigma_i \leq \Sigma_j$. The partially ordered set $(\mathcal{S}, \leq)$ is called the *lattice of isotropy subgroups* of the Γ action on V [6]. The *diagram* of the lattice of isotropy subgroups is a directed graph with vertices S_i and arrows $S_i \leftarrow S_j$ if, and only if, $S_i \lneq S_j$ and there is no symmetry type between S_i and S_j. The diagram of the isotropy lattice of the $\mathbb{D}_6 \times \mathbb{Z}_2$ action on $L^2(\Omega)$ is shown in condensed form in Figure 2.

Irreducible Representations and the Isotypic Decomposition. In order to understand the symmetry-breaking bifurcations we need to first understand irreducible representations and the isotypic decomposition of a group action. The information about the irreducible representations is summarized in character tables [23, 25, 26, 28]. For our purposes, irreducible representations over the field $\mathbb{R}$ are required, see [6, 7]. The *irreducible representations of* Γ are homomorphisms from Γ to the space of $d_j \times d_j$ real matrices: $\gamma \mapsto \alpha^{(j)}(\gamma)$, such that no proper subspace of $\mathbb{R}^{d_j}$ is invariant under $\alpha^{(j)}(\gamma)$ for all $\gamma \in \Gamma$. The *dimension of the irreducible representation* $\alpha^{(j)}$ is d_j. We call $W \subseteq V$ a Γ-*invariant subspace of* V if $\Gamma \cdot W \subseteq W$. An *irreducible subspace of* V is an invariant subspace with no proper invariant subspaces. Every irreducible subspace of the Γ action on V corresponds to a unique (up to similarity) irreducible representation of Γ. The dimension of the irreducible subspace is the same as the dimension of the corresponding irreducible representation.

For each irreducible representation $\alpha^{(j)}$ of Γ, the *isotypic component* of V for the Γ action, denoted by $V_\Gamma^{(j)}$, is defined to be the direct sum of all of the irreducible subspaces corresponding to the fixed $\alpha^{(j)}$ [6, 7, 20]. The *isotypic decomposition* of V is then

$$V = \bigoplus_j V_\Gamma^{(j)}. \tag{14}$$

Some of the isotypic components might be the single point at the origin. These can be left out of the isotypic decomposition. A description of the isotypic components in terms of projection operators is given in [20].

For any group Γ, we denote the trivial representation by $\alpha^{(1)}$. That is $\alpha^{(1)}(\gamma) = 1$ for all $\gamma \in \Gamma$. Thus, if Γ is an isotropy subgroup of a Γ_0 action on V, then

$$V_\Gamma^{(1)} = \mathrm{Fix}(\Gamma, V).$$

Example 4.8. Let us consider the $\mathbb{D}_6 = \langle \rho, \sigma, \tau \rangle$ action on $L^2(\Omega)$. We need to consider the six irreducible representations of $\mathbb{D}_6$, which are listed in [20], to find the isotypic decomposition of $L^2(\Omega)$. Since these isotypic components are central to our problem, we drop the $\mathbb{D}_6$ and define $V^{(j)} := V_{\mathbb{D}_6}^{(j)}$, $j = 1, 2, \ldots, 6$ as follows:

$$\begin{aligned}
V^{(1)} &= \{u \in L^2(\Omega) \mid \rho \cdot u = u,\ \sigma \cdot u = u,\ \tau \cdot u = u\} \\
V^{(2)} &= \{u \in L^2(\Omega) \mid \rho \cdot u = u,\ \sigma \cdot u = -u,\ \tau \cdot u = -u\} \\
V^{(3)} &= \{u \in L^2(\Omega) \mid \rho \cdot u = -u,\ \sigma \cdot u = u,\ \tau \cdot u = -u\} \\
V^{(4)} &= \{u \in L^2(\Omega) \mid \rho \cdot u = -u,\ \sigma \cdot u = -u,\ \tau \cdot u = u\} \\
V^{(5)} &= \{u \in L^2(\Omega) \mid \rho^3 \cdot u = u,\ u + \rho^2 \cdot u + \rho^4 \cdot u = 0\} \\
V^{(6)} &= \{u \in L^2(\Omega) \mid \rho^3 \cdot u = -u,\ u + \rho^2 \cdot u + \rho^4 \cdot u = 0\}.
\end{aligned} \tag{15}$$

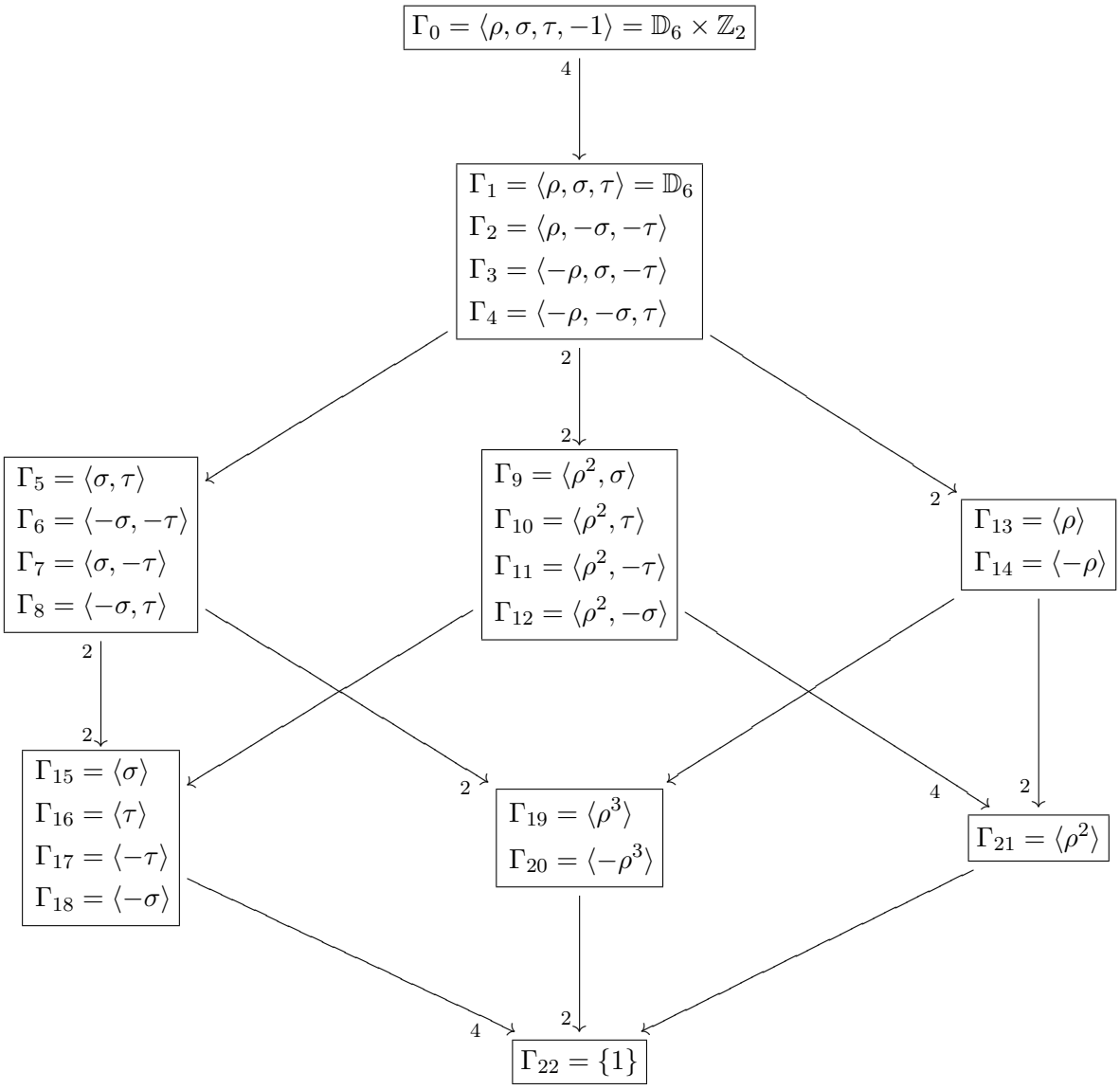

FIGURE 2. The condensed diagram of the isotropy lattice (see [6]) for the $\mathbb{D}_6 \times \mathbb{Z}_2$ action on $L^2(\Omega)$. The vertices of this diagram are the symmetry types (equivalence classes of isotropy subgroups). We follow the convention [6, 7] that one element Γ_i of each symmetry type $S_i = [\Gamma_i]$ is listed. The representatives Γ_i have the property that $\Gamma_i \leq \Gamma_j$ iff $S_i \leq S_j$. Contour plots of solutions to PDE (1) with each of the 23 symmetry types are given in Figures 13 and 14. The diagram of the isotropy lattice is condensed as in [26]. The small numbers on the edges tell the number of connections emanating from each symmetry type in a box. A missing small number means 1. For example, the two arrows representing $[\Gamma_{21}] \leq [\Gamma_{13}]$ and $[\Gamma_{21}] \leq [\Gamma_{14}]$ in the full diagram are collapsed to a single arrow in the condensed diagram. For Γ_0 through Γ_4, the τ generator is redundant since $\tau = \rho^3\sigma$, but its presence makes the subgroups manifest. For example, $\Gamma_2 = \langle \rho, -\sigma, -\tau \rangle = \langle \rho, -\sigma \rangle$, but the three generators make it clear that $\langle -\sigma, -\tau \rangle \leq \langle \rho, -\sigma, -\tau \rangle$.

The last two components are subdivided in terms of a "canonical basis" as $V^{(5)} = V_1^{(5)} \oplus V_2^{(5)}$ and $V^{(6)} = V_1^{(6)} \oplus V_2^{(6)}$, where

$$
\begin{aligned}
V_1^{(5)} &= \{u \in V^{(5)} \mid \sigma \cdot u = u,\ \tau \cdot u = u\} \\
V_2^{(5)} &= \{u \in V^{(5)} \mid \sigma \cdot u = -u,\ \tau \cdot u = -u\} \\
V_1^{(6)} &= \{u \in V^{(6)} \mid \sigma \cdot u = u,\ \tau \cdot u = -u\} \\
V_2^{(6)} &= \{u \in V^{(6)} \mid \sigma \cdot u = -u,\ \tau \cdot u = u\}.
\end{aligned} \tag{16}
$$

As described in [20], the canonical basis corresponds to a particular choice of the irreducible representation $\alpha^{(5)}$ or $\alpha^{(6)}$ within its equivalence class.

Example 4.9. Now, let us consider the isotypic decomposition of the $\Gamma_5 = \langle \sigma, \tau \rangle \cong \mathbb{Z}_2 \times \mathbb{Z}_2$ action on $L^2(\Omega)$. There are 4 irreducible representations of $\mathbb{Z}_2 \times \mathbb{Z}_2$, each of which is one-dimensional. The trivial representation is $\alpha^{(1)}$, and the others are defined by $\alpha^{(2)}(\sigma) = -1$, $\alpha^{(2)}(\tau) = -1$, $\alpha^{(3)}(\sigma) = 1$, $\alpha^{(3)}(\tau) = -1$, $\alpha^{(4)}(\sigma) = -1$, and $\alpha^{(4)}(\tau) = 1$. The four isotypic components of $L^2(\Omega)$ for the Γ_5 action, written in terms of the spaces defined in (15) and (16), are

$$
\begin{aligned}
V^{(1)}_{\langle \sigma,\tau \rangle} &= \{u \in L^2(\Omega) \mid \sigma \cdot u = u, \tau \cdot u = u\} &&= V^{(1)} \oplus V_1^{(5)} \\
V^{(2)}_{\langle \sigma,\tau \rangle} &= \{u \in L^2(\Omega) \mid \sigma \cdot u = -u, \tau \cdot u = -u\} &&= V^{(2)} \oplus V_2^{(5)} \\
V^{(3)}_{\langle \sigma,\tau \rangle} &= \{u \in L^2(\Omega) \mid \sigma \cdot u = u, \tau \cdot u = -u\} &&= V^{(3)} \oplus V_1^{(6)} \\
V^{(4)}_{\langle \sigma,\tau \rangle} &= \{u \in L^2(\Omega) \mid \sigma \cdot u = -u, \tau \cdot u = u\} &&= V^{(4)} \oplus V_2^{(6)}.
\end{aligned}
$$

Note that the canonical basis introduced in [20] is needed for an efficient description of the isotypic decomposition. This is one example of how the canonical basis is the best basis of eigenfunctions to use with the GNGA.

Example 4.10. The isotypic decomposition of $\Gamma_{13} = \langle \rho \rangle \cong \mathbb{Z}_6$ illustrates some features of *real* representation theory. The irreducible representations of $\mathbb{Z}_6$ over $\mathbb{C}$ are all one-dimensional. They are $\alpha^{(j)}(\rho) = (e^{i\pi/3})^{j-1}$ for $j = 1, 2, \ldots, 6$. Over the field $\mathbb{R}$, however, the one-dimensional irreducible representations of $\mathbb{Z}_6$ are given by

$$
\alpha^{(1)}(\rho) = 1, \quad \alpha^{(2)}(\rho) = -1, \tag{17}
$$

and the two-dimensional irreducible representations of $\mathbb{Z}_6$, up to similarity transformations, are given by

$$
\alpha^{(3)}(\rho) = \begin{pmatrix} -\frac{1}{2} & \frac{\sqrt{3}}{2} \\ -\frac{\sqrt{3}}{2} & -\frac{1}{2} \end{pmatrix}, \quad \alpha^{(4)}(\rho) = \begin{pmatrix} \frac{1}{2} & \frac{\sqrt{3}}{2} \\ -\frac{\sqrt{3}}{2} & \frac{1}{2} \end{pmatrix}. \tag{18}
$$

Note that $\alpha^{(3)}(\rho)$ is matrix for a rotation by 120° and $\alpha^{(4)}(\rho)$ is a 60° rotation matrix.

An irreducible representation over $\mathbb{R}$ is called *absolutely irreducible* if it is also irreducible over $\mathbb{C}$. For example, all of the irreducible representations of $\mathbb{D}_6$ listed in [20] are absolutely irreducible, as are the one-dimensional irreducible representations of $\mathbb{Z}_6$ in equation (17). On the other hand, the two-dimensional irreducible representations of $\mathbb{Z}_6$ in equation (18) are *not* absolutely irreducible.

The four isotypic components of the $\langle \rho \rangle$ action on $L^2(\Omega)$ are

$$
V^{(1)}_{\langle \rho \rangle} = \{u \in L^2(\Omega) \mid \rho \cdot u = u\} = V^{(1)} \oplus V^{(2)}
$$

$$
V^{(2)}_{\langle \rho \rangle} = \{u \in L^2(\Omega) \mid \rho \cdot u = -u\} = V^{(3)} \oplus V^{(4)}
$$

$$
V^{(3)}_{\langle \rho \rangle} = V^{(5)}, \text{ and } V^{(4)}_{\langle \rho \rangle} = V^{(6)}.
$$

If we had used the complex irreducible representations, some of the corresponding isotypic components would contain complex-valued functions. It is more natural to use real irreducible representations, and consider only real-valued functions. The price we pay is that most of the representation theory found in books, and built into GAP, is done for complex irreducible representations.

As illustrated by these examples, the isotypic decomposition for each of the 23 isotropy subgroups of $\mathbb{D}_6 \times \mathbb{Z}_2$ can be written as a direct sum of some subset of the eight spaces $V^{(j)}$, for $j = 1, \ldots, 4$, and $V_1^{(j)}$ and $V_2^{(j)}$ for $j = 5, 6$ defined in (15) and (16). Example 4.9 shows that the subdivision of $V^{(5)}$ and $V^{(6)}$, described in (16), is needed. This is the reason why we prefer the canonical basis described in [20], which was not used in [11]. Each of the eigenfunctions is an element of one of these eight spaces, and this information is known by the C++ program. The $\mathbb{D}_6 \times \mathbb{Z}_2$ action on the Galerkin space $B_M = \{\sum_{i=1}^{M} a_i \psi_i\} \cong \mathbb{R}^M$ is quite simple. For example,

$$V_1^{(5)} \cap B_M = \left\{ \sum_{i=1}^{M} a_i \psi_i \mid a_i = 0 \text{ if } \psi_i \notin V_1^{(5)} \right\}.$$

Thus, the C++ program can easily check if a function is in any of the isotypic components $V_{\Gamma_i}^{(j)}$ of B_M for each of the Γ_i, $i = 0, 1, \ldots, 22$, actions.

Symmetry-Breaking Bifurcations. The fact that there are 23 *possible* symmetry types of solutions to the PDE (1) begs the question, do solutions with each of these symmetry types exist? Clearly the trivial solution $u = 0$, with symmetry type S_0, exits. Our procedure for finding approximate solutions with each of these symmetry types is to start with the trivial solution and recursively follow solution branches created at symmetry-breaking bifurcations.

Let us start by abstracting the PDE defined by (1), which depends on the real parameter λ. Let V be an inner product space and $J : \mathbb{R} \times V \to \mathbb{R}$ be a family of Γ_0-invariant functions that depends on a parameter λ. That is, $J(\lambda, \gamma \cdot u) = J(\lambda, u)$ for all $\gamma \in \Gamma_0$ and $u \in V$. It is understood that Γ_0 is the *largest* known group for which J is invariant; of course J is also invariant under any subgroup of Γ_0. We will use Γ, or Γ_i, to refer to an isotropy subgroup of the "full" group Γ_0. Consider the steady-state bifurcation problem $g(\lambda, u) = 0$, where $g(\lambda, u) = \nabla J(\lambda, u)$. Throughout this paper, the gradient ∇ acts on the u component. Note that $g : \mathbb{R} \times V \to V$ is a family of Γ_0-equivariant gradient operators on V. That is, $g(\lambda, \gamma \cdot u) = \gamma \cdot g(\lambda, u)$. In our PDE, we can take g as in (6), or consider (possibly restricted and/or projected) gradients of the functional J from (5) on B_M, H, or other subspaces of L^2 (see Section 2). We can even think of the underlying vector space as the collection of functions on a grid, which is isomorphic to $\mathbb{R}^N$, as we do when using GAP to generate usable isotropy and bifurcation information. In any case, for our snowflake region and odd nonlinearity f the largest known symmetry group is $\Gamma_0 = \mathbb{D}_6 \times \mathbb{Z}_2$.

We define a *branch of solutions* to be the set $\{(\lambda, u) \in \mathbb{R} \times L^2(\Omega) \mid g(\lambda, u) = 0\}$ where the functions u are solutions with a fixed isotropy subgroup. A branch of solutions B_1 has a *symmetry-breaking bifurcation* at the *bifurcation point* $(\lambda^*, u^*) \in B_1$ if a branch of solutions, B_2, with a different isotropy subgroup, has (λ^*, u^*) as a limit point but $(\lambda^*, u^*) \notin B_2$. We say that branch B_2 is *created* at this bifurcation, and often refer to B_1 as the *mother branch* and B_2 as the *daughter branch*. The isotropy subgroup of the daughter branch is always a subgroup of the isotropy subgroup of the mother branch. That is, the daughter has less symmetry than the mother. Our goal in this section is to deduce what we can, from symmetry considerations alone, about the branches created at the bifurcation.

The main tool for finding bifurcation points is the Hessian of the energy functional, the linear map $h(\lambda, u) : V \to V$ defined by $h(\lambda, u) = D^2 J(\lambda, u) = D_u g(\lambda, u)$. The Hessian represents $J''(u)$ (for λ fixed) in that $J''(u)(v, w) = \langle h(u)v, w \rangle$ for all $v, w \in V$. The Hessian is a symmetric linear map, i.e., $\langle h(u)v, w \rangle = \langle v, h(u)w \rangle$. In Section 2, the vector g and the matrix h represent these objects in the coefficient space B_M. If (λ^*, u^*) is a bifurcation point, then $h(\lambda^*, u^*)$ is not invertible, since otherwise the implicit function theorem would guarantee the existence of a unique local solution

branch. The solutions to $g(\lambda, u) = 0$ are critical points of J, so we use the terms solution and critical point interchangeably.

Example 4.11. The trivial solution to (1, 2) is $u = 0$, and the *trivial branch* is $\{(\lambda, 0) \mid \lambda \in \mathbb{R}\}$. Since $h(\lambda, 0)(v) = \Delta v + \lambda v$, the bifurcation points of the trivial branch are $(\lambda_i, 0)$, where $\lambda_i, i \in \mathbb{N}$ are the eigenvalues of the Laplacian on Ω with 0 Dirichlet boundary condition. The i-th *primary branch* is created at the bifurcation point $(\lambda_i, 0)$ on the trivial branch. In cases with double eigenvalues, for example $\lambda_2 = \lambda_3$, there are two branches created at the same point. Near $(\lambda_i, 0)$, the solutions on the i-th primary branch are approximately some constant times the i-th eigenfunctions of the Laplacian, ψ_i.

We define a *degenerate critical point*, or a *degenerate solution*, to be a point (λ^*, u^*) which satisfies $g(\lambda^*, u^*) = 0$ and $\det h(\lambda^*, u^*) = 0$. Thus, every bifurcation point is a degenerate critical point. Some degenerate critical points are not bifurcation points. For example, when a branch folds over and is not monotonic in λ, the *fold point* is degenerate, but is not a bifurcation point as we have defined it. (Note that we avoid the term "saddle-node bifurcation" since there is really no bifurcation.)

The *Morse index* (MI) of a critical point (λ^*, u^*) is defined to be the number of negative eigenvalues of $h(\lambda^*, u^*) = D^2 J(\lambda^*, u^*)$, provided no eigenvalue is 0. The Hessian is symmetric, so all of its eigenvalues are real. The Morse index is undefined at a degenerate critical point, and the MI on a branch of solutions typically changes at a bifurcation point. We will ignore the rare cases where the Morse index is the same on both sides of a degenerate critical point, and we will assume that the degenerate critical points are isolated. In particular, we assume that the group Γ_0 is finite, e.g., $\mathbb{D}_6 \times \mathbb{Z}_2$. If Γ_0 is infinite, then some critical points lie on manifolds with the same dimension as Γ_0. These critical points are always degenerate since infinitesimal motions in Γ_0 correspond to eigenvectors of $D^2 J(\lambda^*, u^*)$ with zero eigenvalue. The GNGA can handle such cases (see the works in progress [21, 27]).

Let us develop some notation to talk about bifurcations. Suppose that (λ^*, u^*) is an isolated degenerate critical point of a Γ_0-equivariant system $g(\lambda, u) = 0$, where Γ_0 is the largest known symmetry group of the system. Let $\Gamma = \mathrm{Stab}(u^*, \Gamma_0)$, and define $L := h(\lambda^*, u^*)$. If we translate u^* to the origin the system becomes $g(\lambda, u - u^*) = 0$ which is Γ-equivariant but not Γ_0-equivariant. Thus Γ, not Γ_0, is important as far as the bifurcation of (λ^*, u^*) is concerned. Let E be the null space of the Γ-equivariant operator L. We call E the *center eigenspace*. Let Γ' be the point stabilizer of E. The definitions are repeated here for reference:

$$\Gamma := \mathrm{Stab}(u^*, \Gamma_0),\ L := h(\lambda^*, u^*),\ E := N(L),\ \Gamma' := \mathrm{pStab}(E, \Gamma), \tag{19}$$

where it is understood that (λ^*, u^*) is an isolated degenerate critical point: $\Gamma_0 \cdot u^*$ is a finite set, $g(\lambda^*, u^*) = 0$ and L is singular.

If $e \in E$, then $L(e) = 0$ by definition. For any $\gamma \in \Gamma$, $\gamma \cdot e \in E$ since the Γ-equivariance of L implies that $L(\gamma \cdot e) = \gamma \cdot L(e) = 0$. Hence,

$$\mathrm{Stab}(E, \Gamma) = \Gamma.$$

Note that $\mathrm{Stab}(E, \Gamma)/\,\mathrm{pStab}(E, \Gamma) = \Gamma/\Gamma'$ acts faithfully on E. In the usual case where (λ^*, u^*) is a bifurcation point, not just a degenerate critical point, we say that Γ/Γ' is the *symmetry group of the bifurcation*, or that (λ^*, u^*) undergoes a *bifurcation with* Γ/Γ' *symmetry*.

Example 4.12. Consider a degenerate critical point (λ^*, u^*) of the PDE (1, 2) with isotropy subgroup $\Gamma = \mathbb{D}_6 = \langle \rho, \sigma \rangle$. Only Γ, and not $\Gamma_0 = \mathbb{D}_6 \times \mathbb{Z}_2$, is important as far as bifurcations of (λ^*, u^*) are concerned. Let E be the null space of $L = h(\lambda^*, u^*)$. As we will explain later, there are six generic possibilities for $\Gamma' = \mathrm{pStab}(E, \Gamma)$ when $\Gamma = \mathbb{D}_6$. One possibility is that $\Gamma' = \langle \rho \rangle$, which gives $\Gamma/\Gamma' \cong \mathbb{Z}_2$. Thus, (λ^*, u^*) can undergo a bifurcation with $\mathbb{Z}_2$ symmetry. We emphasize that $\mathrm{pStab}(E, \Gamma)$, not $\mathrm{pStab}(E, \mathbb{D}_6 \times \mathbb{Z}_2)$, is important since the bifurcation of (λ^*, u^*) involves the affine subspace $u^* + E \subseteq L^2(\Omega)$, and $\mathrm{pStab}(u^* + E, \mathbb{D}_6 \times \mathbb{Z}_2) = \mathrm{pStab}(E, \Gamma) = \langle \rho \rangle$. In this case $\mathrm{pStab}(E, \mathbb{D}_6 \times \mathbb{Z}_2) = \langle \rho, -\sigma, -\tau \rangle$ is not relevant.

In the notation of (19), L sends each of the isotypic components $V_\Gamma^{(j)}$ to itself [20, 25, 28]. Barring "accidental degeneracy," the center eigenspace E is a Γ-irreducible subspace. Thus, E is typically a subspace of exactly one isotypic component $V_\Gamma^{(j)}$, and $\dim(E)$ is the dimension d_j of the corresponding corresponding irreducible representation, $\alpha^{(j)}$. Furthermore, the point stabilizer of E is the kernel of $\alpha^{(j)}$ and can be computed without knowing E. In summary, the following typically holds for the center eigenspace at a degenerate critical point with isotropy subgroup Γ:

$$E \subseteq V_\Gamma^{(j)} \text{ for some } j, \quad \dim(E) = \Delta MI = d_j, \quad \text{and } \Gamma' = \{\gamma \in \Gamma \mid \alpha^{(j)}(\gamma) = I\}.$$

Accidental degeneracy is discussed in [20, 25, 28]. We did not encounter any accidental degeneracy in our numerical investigation of (1, 2), so we will not discuss it further here.

We finally have the background to describe the bifurcations which occur in equivariant systems. The goal is to predict what solutions will be created at each of the symmetry breaking bifurcations, and know what vectors in E to use to start these branches using the pmGNGA. While such a prediction is impossible in general, we can determine how to follow all of the bifurcating branches in the system (1, 2). We follow the treatment and notation of [6, 7]. At a symmetry-breaking bifurcation we can translate (λ^*, u^*) to the origin, and we could, in principle, do an equivariant Liapunov-Schmidt reduction or center manifold reduction to obtain reduced bifurcation equations $\tilde{g} : \mathbb{R} \times E \to E$ where $\tilde{g}(0,0) = 0$, $D\tilde{g}(0,0) = 0$, and $\tilde{g}$ is $\Gamma := \mathrm{Stab}(u^*)$-equivariant. It is important to realize that we do not actually need to perform the Liapunov-Schmidt reduction.

The most powerful tool for understanding symmetry breaking bifurcations is the Equivariant Branching Lemma. Recall that absolutely irreducible representations were defined in Example 4.10. See [6, 7] for a thorough discussion of the Equivariant Branching Lemma, including further references.

Theorem 4.13. Equivariant Branching Lemma (EBL) *Suppose Γ acts absolutely irreducibly on the space E, and let $\tilde{g} : \mathbb{R} \times E \to E$ be Γ-equivariant. Assume that Γ acts nontrivially, so $\tilde{g}(\lambda, 0) = 0$. Since Γ acts absolutely irreducibly, $D\tilde{g}(\lambda, 0) = c(\lambda)I_d$ for some function $c : \mathbb{R} \to \mathbb{R}$, where I_d is the identity matrix of size $d = \dim(E)$. Assume that $c(0) = 0$ and $c'(0) \neq 0$. Let Σ be an isotropy subgroup of the Γ action on E with $\dim \mathrm{Fix}(\Sigma, E) = 1$. Then there are at least two solutions branches of $\tilde{g}(\lambda, u) = 0$ with isotropy subgroup Σ created at $(0, 0)$.*

The EBL, combined with Liapunov-Schmidt theory, implies that there are at least two solutions branches of the full problem $g(\lambda, u) = 0$ with isotropy subgroup Σ created at the bifurcation point (λ^*, u^*). We call these newly created branches *EBL branches* since their existence can be predicted by the EBL. Other branches created at a bifurcation are called *non-EBL branches*.

Following [6, 7], we define a *maximal isotropy subgroup* of a Γ action on V to be an isotropy subgroup $\Sigma \neq \Gamma$ with the property that if Θ is an isotropy subgroup such that $\Sigma \leq \Theta$, then $\Theta = \Sigma$ or $\Theta = \Gamma$. In other words, a maximal isotropy subgroup is a maximal proper isotropy subgroup. In the context of the EBL, if $\dim(\mathrm{Fix}(\Sigma, E)) = 1$, then Σ is a maximal isotropy subgroup of the Γ action on E. The converse, however, is not true.

In gradient systems, for example the PDE (1, 2), more can be said. If Σ is any maximal isotropy subgroup of the Γ action on E, then there is typically a solution branch created at the bifurcation with isotropy subgroup Σ. If $\dim \mathrm{Fix}(\Sigma, E) \geq 2$, the branch created is an example of a *non-EBL* branch. See [6, 7, 24] for a discussion of bifurcations in gradient systems.

As discussed in Proposition 4.5, if Σ is any isotropy subgroup of the Γ action on E, then the stabilizer of $\mathrm{Fix}(\Sigma, E)$ is $N_\Gamma(\Sigma)$. Equation (12) reminds us that the point stabilizer of $\mathrm{Fix}(\Sigma, E)$ is Σ. Therefore, the effective symmetry group of $\tilde{g}$, restricted to $\mathrm{Fix}(\Sigma, E)$, is $N_\Gamma(\Sigma)/\Sigma$.

Example 4.14. Consider a degenerate critical point with isotropy subgroup $\Gamma_1 = \mathbb{D}_6 = \langle \rho, \sigma, \tau \rangle$. Barring accidental degeneracy, the center eigenspace E is a subspace of one of the 6 isotypic components of the $\mathbb{D}_6$ action on $L^2(\Omega)$ described in Example 4.8. Figure 3 shows the lattice of isotropy subgroups for $\mathbb{D}_6$ acting on each of these 6 isotypic components $V^{(j)}$. These 6 cases can be distinguished by determining which isotypic component any eigenfunction in E belongs to. We shall

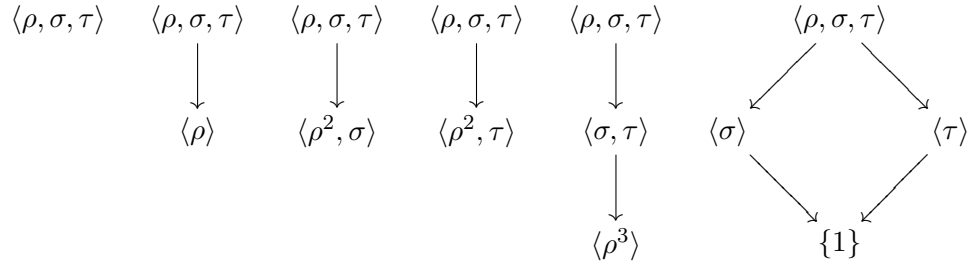

FIGURE 3. Diagrams of the six isotropy lattices for the actions of $\mathbb{D}_6 = \langle \rho, \sigma, \tau \rangle$ on each of the six isotypic components $V^{(j)}$ of the $\mathbb{D}_6$ action on $L^2(\Omega)$. This describes the six possibilities (barring accidental degeneracy) for the $\mathbb{D}_6$ action on the center eigenspace E at a degenerate critical point.

go through each of these six cases, and describe the resulting bifurcation. Recall that $\Gamma = \Gamma_1 = \mathbb{D}_6$ for each of these cases. The minimal isotropy subgroup in each case is $\Gamma' = \mathrm{pStab}(E, \Gamma)$. The cases are

$$\begin{aligned}
E \subseteq V^{(1)} \Rightarrow &\quad \Gamma' = \Gamma_1 = \langle \rho, \sigma, \tau \rangle, \quad \dim E = 1, \quad \Gamma/\Gamma' \cong \{1\} \\
E \subseteq V^{(2)} \Rightarrow &\quad \Gamma' = \Gamma_{13} = \langle \rho \rangle, \qquad\quad \dim E = 1, \quad \Gamma/\Gamma' \cong \mathbb{Z}_2 \\
E \subseteq V^{(3)} \Rightarrow &\quad \Gamma' = \Gamma_9 = \langle \rho^2, \sigma \rangle, \qquad \dim E = 1, \quad \Gamma/\Gamma' \cong \mathbb{Z}_2 \\
E \subseteq V^{(4)} \Rightarrow &\quad \Gamma' = \Gamma_{10} = \langle \rho^2, \tau \rangle, \qquad \dim E = 1, \quad \Gamma/\Gamma' \cong \mathbb{Z}_2 \\
E \subseteq V^{(5)} \Rightarrow &\quad \Gamma' = \Gamma_{19} = \langle \rho^3 \rangle, \qquad \dim E = 2, \quad \Gamma/\Gamma' \cong \mathbb{D}_3 \\
E \subseteq V^{(6)} \Rightarrow &\quad \Gamma' = \Gamma_{22} = \{1\}, \qquad\quad \dim E = 2, \quad \Gamma/\Gamma' \cong \mathbb{D}_6.
\end{aligned}$$

The first case, $E \subseteq V^{(1)} = \mathrm{Fix}(\Gamma_1, L^2(\Omega))$, does not lead to a symmetry-breaking bifurcation. The $\mathbb{D}_6$ action on E is trivial, so the EBL does not apply. The degenerate critical point (u^*, λ^*) is typically a fold point (or saddle-node), not a bifurcation point. In the neighborhood of the fold point there is only one solution branch, with isotropy subgroup Γ_1, and the branch lies to one side of $\lambda = \lambda^*$ or the other.

The next three cases, with $\Gamma/\Gamma' \cong \mathbb{Z}_2$ symmetry, are called *pitchfork bifurcations*. Clearly, the only maximal isotropy subgroup is Γ' in each case, and the EBL applies. The effective symmetry group acting on E is $\mathbb{Z}_2$, so there are two conjugate solution branches created at the bifurcation. In the branch following code we follow one of these branches using the pmGNGA starting with any eigenvector $e \in E$.

The next case, with $E \subseteq V^{(5)}$, is a bifurcation with $\mathbb{D}_3$ symmetry. There is a maximal isotropy subgroup Γ_5 which is different from $\Gamma' = \Gamma_{19}$ in this case. It satisfies

$$\dim \mathrm{Fix}(\Gamma_5, E) = 1, \text{ and } N_{\Gamma_1}(\Gamma_5)/\Gamma_5 = \{1\}.$$

Using a projection operator, we can find an eigenvector $e \in E$ with $\mathrm{Stab}(e, \Gamma_1) = \Gamma_5$. The pmGNGA using this eigenvector e will follow one of the solution branches created at the bifurcation, and the pmGNGA using the negative eigenvector $-e$ will find a branch that is not conjugate to the first. From our knowledge of bifurcations with $\mathbb{D}_3$ symmetry (see [6, 7]) we know that typically only these two branches (and their Γ_1 group orbits) are created at the bifurcation. (There are six branches created in all.) We also know that the branches are *transcritical*, meaning that one branch exists for $\lambda < \lambda^*$ and the other exists for $\lambda > \lambda^*$.

The last case, with $E \subseteq V^{(6)}$, is a bifurcation with $\mathbb{D}_6$ symmetry. There are two maximal symmetry types, the conjugacy classes of Γ_{15} and Γ_{16}. A calculation shows that

$$\dim \mathrm{Fix}(\Gamma_{15}, E) = \dim \mathrm{Fix}(\Gamma_{16}, E) = 1, \text{ and } N_{\Gamma_1}(\Gamma_{15})/\Gamma_{15} = N_{\Gamma_1}(\Gamma_{16})/\Gamma_{16} = \{1\}.$$

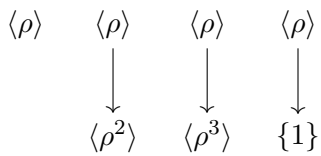

FIGURE 4. The diagrams of the four isotropy lattices for the actions of $\Gamma_{13} = \langle\rho\rangle$ on each of the four isotypic components $V^{(j)}_{\langle\rho\rangle}$ of the Γ_{13} action on $L^2(\Omega)$. This describes the four possibilities (barring accidental degeneracy) for the Γ_{13} action on the center eigenspace E at a degenerate critical point.

To follow one branch from each of the group orbits of solution branches created at this bifurcation, it suffices to use the pmGNGA twice, with the eigenvectors $e_1, e_2 \in E$, where $\mathrm{Stab}(e_1, \Gamma_1) = \Gamma_{15}$ and $\mathrm{Stab}(e_2, \Gamma_1) = \Gamma_{16}$. It is well-known that these EBL-branches are typically the only branches created at a bifurcation with $\mathbb{D}_6$ symmetry [6, 7].

Example 4.15. Consider a degenerate critical point with isotropy subgroup $\Gamma_{13} = \langle\rho\rangle \cong \mathbb{Z}_6$. Barring accidental degeneracy, the center eigenspace E is a subspace of one of the 4 isotypic components $V^{(j)}_{\langle\rho\rangle}$ defined in Example 4.10. Figure 4 shows the lattice of isotropy subgroups for Γ_{13} acting on each of these 4 isotypic components. Recall that $\Gamma = \Gamma_{13} = \langle\rho\rangle$ for each of these cases, and the minimal isotropy subgroup is $\Gamma' = \mathrm{pStab}(E, \Gamma)$. We shall go through each of the four cases, and describe the resulting bifurcation:

$$\begin{aligned}
E \subseteq V^{(1)}_{\langle\rho\rangle} = V^{(1)} \oplus V^{(2)} &\Rightarrow \Gamma' = \Gamma_{13} = \langle\rho\rangle, \quad \dim E = 1, \quad \Gamma/\Gamma' \cong \{1\} \\
E \subseteq V^{(2)}_{\langle\rho\rangle} = V^{(3)} \oplus V^{(4)} &\Rightarrow \Gamma' = \Gamma_{21} = \langle\rho^2\rangle, \quad \dim E = 1, \quad \Gamma/\Gamma' \cong \mathbb{Z}_2 \\
E \subseteq V^{(3)}_{\langle\rho\rangle} = V^{(5)} &\Rightarrow \Gamma' = \Gamma_{19} = \langle\rho^3\rangle, \quad \dim E = 2, \quad \Gamma/\Gamma' \cong \mathbb{Z}_3 \\
E \subseteq V^{(4)}_{\langle\rho\rangle} = V^{(6)} &\Rightarrow \Gamma' = \Gamma_{22} = \{1\}, \quad \dim E = 2, \quad \Gamma/\Gamma' \cong \mathbb{Z}_6.
\end{aligned}$$

The first two cases are analogous to the first two cases in example 4.14. When $\Gamma/\Gamma' \cong \{1\}$ there is a fold point, but no symmetry breaking bifurcation. There is pitchfork bifurcation when $\Gamma/\Gamma' \cong \mathbb{Z}_2$. The next two cases are interesting because Γ_{13} does not act absolutely irreducibly on E, and the EBL does not apply. In both cases Γ' is a maximal isotropy subgroup.

In the third case, where $E \subseteq V^{(3)}_{\langle\rho\rangle} = V^{(5)}$, every eigenfunction in the 2-dimensional E has isotropy subgroup Γ_{19}. Since we have a gradient system, we know that solution branches with isotropy subgroup Γ_{19} are created at this bifurcation with $\mathbb{Z}_3$ symmetry. The bifurcation is well-understood, and it looks like a bifurcation with $\mathbb{D}_3$ symmetry, except that the "angle" of the bifurcating solutions in the E plane is arbitrary. This means that trial and error is needed. Eigenfunctions with several angles are used to start the pmGNGA. If the angle is wrong, Newton's method will not converge to find the first solution on the branch. When a branch is found for a starting eigenfunction e, then its negative $-e$ is used to find the other solution branch.

In the fourth case, where $E \subseteq V^{(4)}_{\langle\rho\rangle} = V^{(6)}$, every eigenfunction in E has the same isotropy subgroup: $\Gamma_{22} = \{1\}$. Gradient bifurcations with $\mathbb{Z}_6$ symmetry look like bifurcations with $\mathbb{D}_6$ symmetry, except that the angle in the E plane is arbitrary. Again, trial and error is needed to find starting eigenfunctions for which the pmGNGA converges.

The Bifurcation Digraph. There are 23 different isotropy subgroups for the $\mathbb{D}_6 \times \mathbb{Z}_2$ action on $L^2(\Omega)$. Thus, a calculation similar to Examples 4.14 and 4.15 needs to be done for each isotropy subgroup except $\Gamma_{22} = \{1\}$. These were done by hand, and verified with GAP. There are 59 generic symmetry-breaking bifurcations, since there are 59 different isotypic components $V^{(j)}_{\Gamma_i}$ on which Γ_i

acts nontrivially. The amount of information is overwhelming, so we display the essential results in what we call a bifurcation digraph.

Definition 4.16. The *bifurcation digraph* of the Γ_0 action on a real vector space V is a directed graph with labelled arrows. The vertices are the symmetry types (equivalence classes of isotropy subgroups). Given Σ and Γ, two isotropy subgroups of the Γ_0 action on V, we draw an arrow from $[\Gamma]$ to $[\Sigma]$ iff Σ is a maximal isotropy subgroup of the Γ action on some isotypic component $V_\Gamma^{(j)}$ of V. Each arrow has the label Γ/Γ', where Γ' is the kernel of the Γ action on $V_\Gamma^{(j)}$. Furthermore, each arrow is either solid, dashed or dotted. The arrow is

$$\begin{aligned}\text{solid if } &\dim \mathrm{Fix}(\Sigma, E) = 1 \text{ and } N_\Gamma(\Sigma)/\Sigma = \mathbb{Z}_2,\\ \text{dashed if } &\dim \mathrm{Fix}(\Sigma, E) = 1 \text{ and } N_\Gamma(\Sigma)/\Sigma = \{1\}, \text{ and}\\ \text{dotted if } &\dim \mathrm{Fix}(\Sigma, E) \geq 2,\end{aligned}$$

where E is any irreducible subspace contained in $V_\Gamma^{(j)}$.

Note that if $\dim \mathrm{Fix}(\Sigma, E) = 1$, then $N_\Gamma(\Sigma)/\Sigma$ is either $\mathbb{Z}_2$ or $\{1\}$, since these are the only linear group actions on $E \cong \mathbb{R}^1$. Thus, the three arrow types (solid, dashed, and dotted) exhaust all possibilities.

Theorem 4.17. *For a given Γ_0 action on V, every arrow in the diagram of the isotropy lattice is an arrow in the bifurcation digraph.*

Proof. Suppose $[\Gamma] \to [\Sigma]$ is an arrow in the diagram of the isotropy lattice. Then some $\Sigma^* \in [\Sigma]$ is a maximal isotropy subgroup of the Γ action on V. Choose $u^* \in V$ such that $\mathrm{Stab}(u^*, \Gamma) = \Sigma^*$. Such a u^* exists since Σ^* is an isotropy subgroup. Now consider the isotypic decomposition $\{V_\Gamma^{(j)}\}_{j\in J}$ of V. We can write $u^* = \sum_{j\in J} u^{(j)}$, where $u^{(j)} \in V_\Gamma^{(j)}$ are uniquely determined. Let γ be any element of Σ^*. Then $\gamma \cdot u^* = \sum_{j\in J} \gamma \cdot u^{(j)} = u^*$. Since each of the components $V_\Gamma^{(j)}$ is Γ-invariant, $\gamma \cdot u^{(j)} = u^{(j)}$ for each $j \in J$. Thus $\Sigma^* \leq \mathrm{Stab}(u^{(j)}, \Gamma)$ for each $j \in J$. Either $\mathrm{Stab}(u^{(j)}, \Gamma) = \Gamma$ or $\mathrm{Stab}(u^{(j)}, \Gamma) = \Sigma^*$, since Σ^* is a maximal isotropy subgroup of the Γ action on V. If $\mathrm{Stab}(u^{(j)}, \Gamma) = \Gamma$ for all $j \in J$, then $\mathrm{Stab}(u^*, \Gamma) = \Gamma$. But $\mathrm{Stab}(u^*, \Gamma) \neq \Gamma$, so $\mathrm{Stab}(u^{(j)}, \Gamma) = \Sigma^*$ for some $j \in J$, and Σ^* is a maximal isotropy subgroup of the Γ action on this component $V_\Gamma^{(j)}$ of V. Therefore the bifurcation digraph has an arrow from $[\Gamma]$ to $[\Sigma^*] = [\Sigma]$. □

Theorem 4.17 says that the bifurcation digraph is an extension of the diagram of the isotropy lattice. The bifurcation digraph has more arrows, in general. As with the lattice of isotropy subgroups [6, 7], we usually draw a single element Γ of the equivalence class, $[\Gamma]$ as the vertices of the bifurcation digraph.

An arrow from Γ to Σ in the bifurcation digraph indicates that a Γ_0-equivariant gradient system $g(\lambda, u) = 0$ can have a generic symmetry-breaking bifurcation where a mother branch with isotropy subgroup Γ creates a daughter branch with isotropy subgroup Σ. The symmetry group of the bifurcation is Γ/Γ', and the center eigenspace at the bifurcation point is the Γ-irreducible space E. The information encoded in the label and arrow type is used by the heuristics of our branch-following algorithm. A solid arrow indicates that every e in the one-dimensional space $\mathrm{Fix}(\Sigma, E)$ satisfies $\gamma \cdot e = -e$ for some $\gamma \in \Sigma$. Thus, there is typically a pitchfork bifurcation in the space $\mathrm{Fix}(\Sigma, E)$. A dashed arrow indicates that $\gamma \cdot e = e$ for all $e \in \mathrm{Fix}(\Sigma, E)$ and $\gamma \in \Sigma$. A dashed arrow often indicates a *transcritical* bifurcation in the space $\mathrm{Fix}(\Sigma, E)$, meaning that one branch bifurcates to the left ($\lambda < \lambda^*$) and a non-conjugate branch bifurcates to the right ($\lambda > \lambda^*$). A dotted arrow indicates that the EBL does not apply to this bifurcation. As mentioned above, branching of solutions corresponding to a dotted arrow is generic in gradient systems [24, 6]. In bifurcations of non-gradient ODEs, a dotted arrow would indicate that a Hopf bifurcation is to be expected, whereas the solid or dashed lines correspond to the possibility of both stationary bifurcations and Hopf bifurcations. Thus, the bifurcation digraph would be useful for non-gradient systems as well.

In our problem, where $\Gamma_0 = \mathbb{D}_6 \times \mathbb{Z}_2$ acts on $L^2(\Omega)$, the label Γ/Γ' and arrow type are sufficient to characterize the bifurcation completely. For more complicated groups, the label may need to contain more information about the action of Γ on E. For example the label $\Gamma/\Gamma' = \mathbb{S}_4$ would be ambiguous, since $\mathbb{S}_4$ has two faithful irreducible representations with different lattices of isotropy subgroups.

Example 4.18. The bifurcations described in Examples 4.14 and 4.15 lead to several edges in the bifurcation digraph for the $\mathbb{D}_6 \times \mathbb{Z}_2$ action on $L^2(\Omega)$. From Example 4.14, we see that there are six arrows in the bifurcation digraph coming from $[\Gamma_1]$. They are

$$\begin{array}{cccccc} [\Gamma_1] & [\Gamma_1] & [\Gamma_1] & [\Gamma_1] & [\Gamma_1] & [\Gamma_1] \\ \downarrow{\scriptstyle \mathbb{Z}_2} & \downarrow{\scriptstyle \mathbb{Z}_2} & \downarrow{\scriptstyle \mathbb{Z}_2} & \vdots{\scriptstyle \mathbb{D}_3} & \downarrow{\scriptstyle \mathbb{D}_6} & \downarrow{\scriptstyle \mathbb{D}_6} \\ [\Gamma_9] & [\Gamma_{10}] & [\Gamma_{13}] & [\Gamma_5] & [\Gamma_{15}] & [\Gamma_{16}] \, . \end{array}$$

From Example 4.15, we see that there are three edges coming from $[\Gamma_{13}]$. Here we list these vertices with the convention [6, 7] used in the lattice of isotropy subgroups that the vertices are Γ_i rather than $[\Gamma_i]$:

$$\begin{array}{ccc} \Gamma_{13} & \Gamma_{13} & \Gamma_{13} \\ \downarrow{\scriptstyle \mathbb{Z}_2} & \vdots{\scriptstyle \mathbb{Z}_3} & \vdots{\scriptstyle \mathbb{Z}_6} \\ \Gamma_{21} & \Gamma_{19} & \Gamma_{22} \, . \end{array}$$

There are 65 directed edges in the bifurcation digraph for the $\mathbb{D}_6 \times \mathbb{Z}_2$ action on $L^2(\Omega)$. A condensed bifurcation digraph is shown in Figure 5. This digraph is of great help in writing an automated code for branch following. There are only 5 possibilities for the symmetry group of the bifurcation: $\Gamma/\Gamma' = \mathbb{Z}_2$, $\mathbb{Z}_3$, $\mathbb{Z}_6$, $\mathbb{D}_3$, or $\mathbb{D}_6$. The symmetry-breaking bifurcation with each of these symmetries is well understood [6, 7], and each is described briefly in example 4.14 or 4.15

5. Symmetry and Computational Efficiency.

Several modifications of the GNGA (2.1) take advantage of symmetry to speed up the calculations. The symmetry forces many of the components of the gradient and Hessian to be zero. We identified these zero components and avoided doing the time-consuming numerical integrations to compute them. At the start of the C++ program, the isotropy subgroup, Γ_i, of the initial guess is computed. Recall that there are M modes in the Galerkin space B_M, so $\dim(B_M) = M$. Define $M_i := \dim(\mathrm{Fix}(\Gamma_i, B_M))$. In our PDE with $\mathbb{D}_6 \times \mathbb{Z}_2$ symmetry, $\mathrm{Fix}(\Gamma_i, B_M)$ is a coordinate subspace of B_M, so at most M_i of the M components of the gradient (6) are nonzero. The numerical integrations are not done for the components of g which must be zero. Furthermore, $M_i(M_i+1)/2$ rather than $M(M+1)/2$ numerical integrations are needed to compute the part of the Hessian matrix h needed by the GNGA algorithm. Equation (7) says that $h_{j\,k} = \lambda_j \, \delta_{j\,k} - \int_\Omega f'(u)\psi_j\psi_k$. The numerical integration is done only if ψ_j and ψ_k are both in $\mathrm{Fix}(\Gamma_i)$, but the $\lambda_j \, \delta_{jk}$ term is included for all $j \in \{1, \ldots, M\}$ so that the Hessian is nonsingular. We then solve the linear system $h\chi = g$ with M equations and M unknowns. We could solve a reduced system with M_i equations and M_i unknowns, but this would not speed up the algorithm very much since the majority of the execution time is spent doing the numerical integrations. After Newton's method converges to a solution, the full Hessian needs to be calculated in order to compute the MI. Here, too, we can take advantage of the symmetry. Since h is a Γ_i-equivariant operator, the Hessian is block diagonal in the isotypic decomposition of B_M for the Γ_i action. In other words, $h_{j\,k} = 0$ if ψ_j and ψ_k are in different isotypic components $V_{\Gamma_i}^{(j)}$ of B_M.

For example, the isotropy subgroup $\Gamma_1 = \mathbb{D}_6$ has $M_1 = 30$ when $M = 300$. When all of the $M + (M+1)/2 = 45450$ numerical integrations were done it took about 44 seconds on a 1GHz PC to do one iteration of Newton's method at level 5. With the symmetry improvements it takes

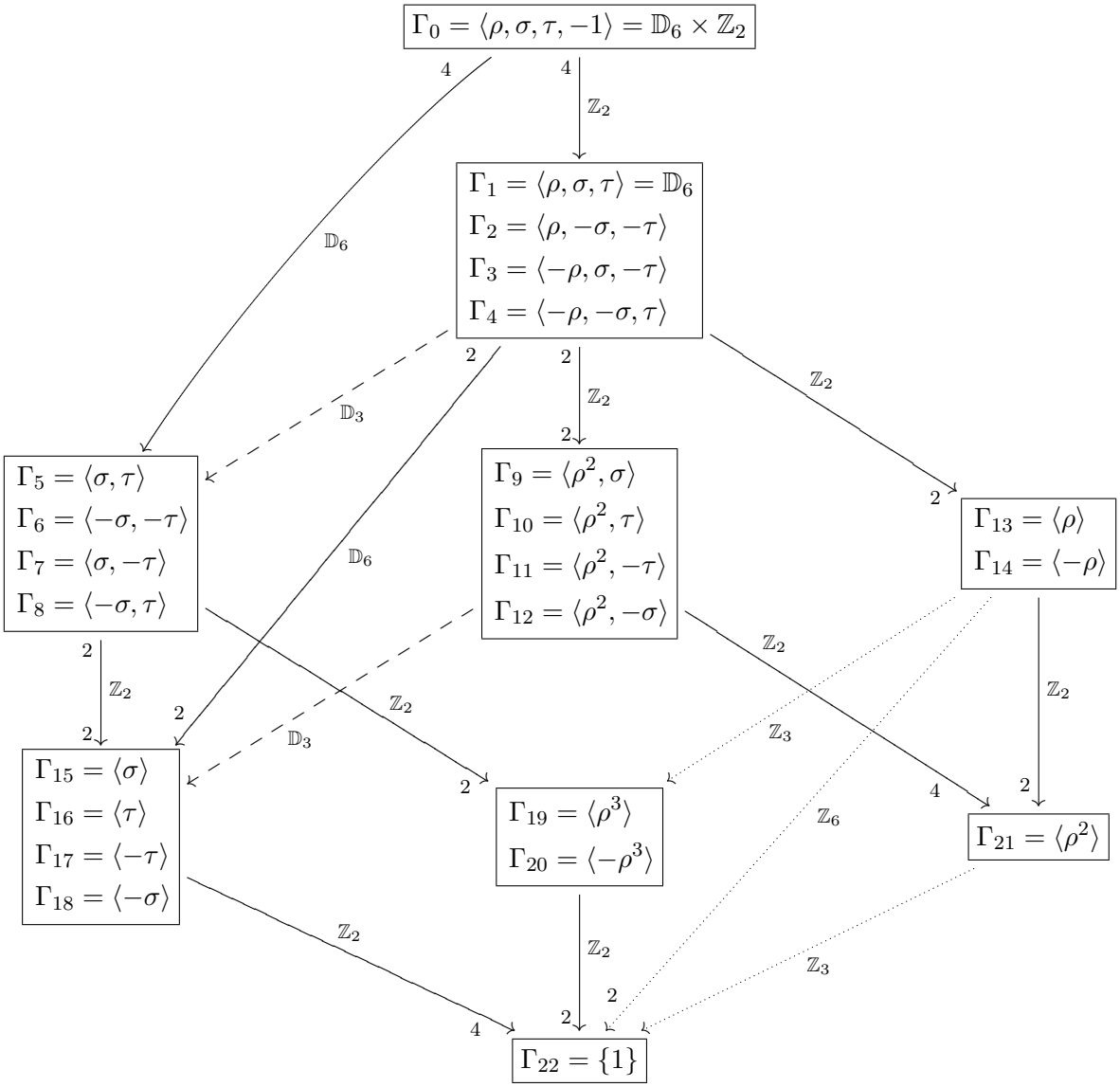

FIGURE 5. The bifurcation digraph for the $\mathbb{D}_6 \times \mathbb{Z}_2$ action on $L^2(\Omega)$ extends the diagram of the isotropy lattice. The digraph shown is condensed as in Figure 2. The arrows indicate generic symmetry breaking bifurcations. The Morse index of the mother branch changes by 1 at bifurcations with $\mathbb{Z}_2$ symmetry, and it changes by 2 at all other bifurcations shown here.

about 1.5 seconds per Newton iteration. The computation of the Hessian restricted to $\mathrm{Fix}(\Gamma_1)$ is about 100 times faster than computing the full Hessian, so we estimate that it took about 43 seconds to compute the 300×300 Hessian doing all the numerical integrations, about 0.5 seconds to compute the 30×30 reduced Hessian, and then about 1 second to solve the linear system $h\chi = g$ for the Newton step χ. After the solution was found, it took about 11 seconds to compute the non-zero elements of the full Hessian and the MI, using the symmetry restrictions to avoid most of the numerical integration. Since Newton's method usually converged in 4 or 5 steps, the C++ program spent more execution time computing the MI than it spent to find the solution, at least for solutions with symmetry type S_1. As the symmetry gets lower on the bifurcation digraph, the program takes more execution time.

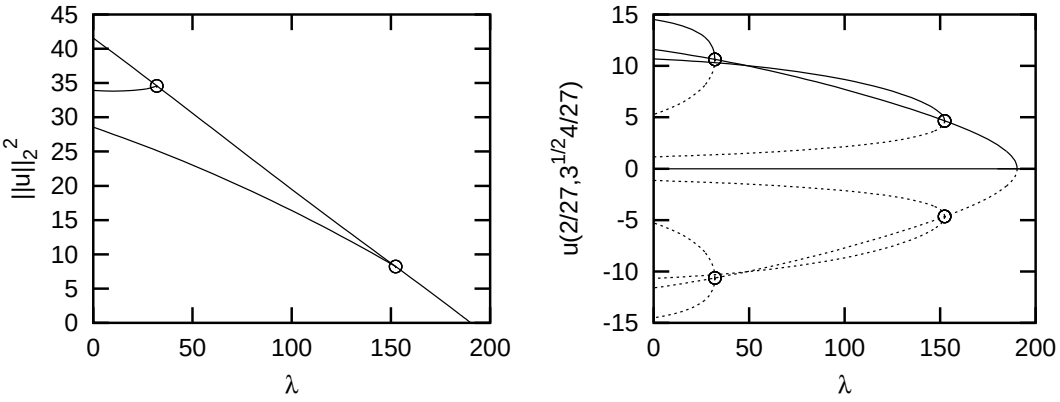

FIGURE 6. Bifurcation diagrams of the sixth primary branch, showing $||u||_2^2$ and $u(2/27, 4\sqrt{3}/27)$ as a function of λ. Since $||u||_2^2$ is a $\mathbb{D}_6 \times \mathbb{Z}_2$-invariant function of u, each group orbit of solution branches is shown as one curve on the left. The disadvantage of plotting $||u||_2^2$ is that the curves in many bifurcation diagrams are not well separated. The point $(2/27, 4\sqrt{3}/27)$ is not on any of the reflection axes of the snowflake region. There are 2 primary branches with symmetry S_1, four secondary branches with symmetry S_9, and four secondary branches with symmetry S_{10}. Our choice for the bifurcation diagrams in this paper combines the advantages of both views: $u(2/27, 4\sqrt{3}/27)$ is plotted as a function of λ for exactly one branch (the solid lines) from each group orbit. Unless indicated otherwise, all figures were produced with level $\ell = 5$ and $M = 300$ modes.

6. Automated Branch Following.

The branch following code is a complex collection of about a dozen Perl scripts, *Mathematica* and Gnuplot scripts, and a C++ program. These programs write and call each other fully automatically and communicate through output files, pipes and command line arguments. A complete bifurcation diagram can be produced by a single call to the main Perl script.

Various choices for the function of u plotted vs. λ are shown in Figure 6. In most bifurcation diagrams we plot approximate solutions u evaluated at a generic point $(2/27, 4\sqrt{3}/27)$ versus the parameter λ; other choices for the vertical axis such as $J(u)$ or $\|u\|_\infty$ lead to less visible separation of branches. Two conjugate solutions can have different values at the generic point, but since our program follows only one branch in each group orbit this does not cause a problem.

The C++ program implements the GNGA algorithm. Its input is a vector of coefficients $a \in \mathbb{R}^M$ for an initial guess in Newton's method, an interval for λ, a stepsize for λ and several other parameters such as the level and the number of modes used in the expansion of solutions. It finds solutions on a single branch of the bifurcation diagram. Every solution is written as a single line in an output file. This line contains all the information about the solution such as the level, the number of modes, the symmetry of the solution, the stepsize, etc. Each line in the output file can be used to write an input file for a subsequent call to the same C++ program.

The C++ program finds one branch (referred to as the main branch) and a short segment of each of the daughter branches created at bifurcations of the main branch. The coefficients approximating the first solution on the branch are supplied to the C++ program. Newton's method is used to find this first solution, then λ is incremented and the next solution is found. The program attempts to follow the main branch all the way to the final λ, usually 0. Heuristics are used to double or halve the λ stepsize when needed, keeping the stepsize in the interval from the initial stepsize (input to the C++ program) to 1/32 of the initial stepsize. For example, the stepsize is halved if Newton's

method does not converge, if it converges to a solution with the wrong symmetry, or if more than one bifurcation is detected in one λ step.

The Morse index is computed at each λ value on the main branch. When the MI changes a subroutine is called to handle the bifurcation before the main branch is continued. If the MI changes from m_1 to m_2, we define $m = \max\{m_1, m_2\}$. Then the bifurcation point is approximated by using the secant method to set the m-th eigenvalue of the Hessian $h(u)$ to zero as a function of λ. The GNGA is needed at each step of the secant method to compute $u = u(\lambda)$. We find that the GNGA works well even though we are approximating a solution for which the Hessian is singular.

After the bifurcation point is approximated, a short segment of each bifurcating branch is computed and one output file is written for each branch. If the Equivariant Branching Lemma (EBL) holds, then we know exactly which critical eigenvector to use for each branch. Let the Fourier coefficients of the solution at the bifurcation point be a^*, let the normalized critical eigenvector be $e \in \mathbb{R}^M$, and let k be defined by $|e_k| \geq |e_i|$ for all i. We then use the pmGNGA with the initial guess $a = a^* + t\,e$, keeping the k-th component fixed and solving for λ and the other $M-1$ components of a. We start with $t = 0.1$, but this is decreased if Newton's method does not converge. More points on the bifurcating branch are computed in the same way, except that a^* is the last solution found on the branch. This short segment of the bifurcating branch ends when λ reaches the bifurcation value λ^* minus the stepsize, or when the pmGNGA does not converge even when t is extremely small, or when a maximum number of points on the branch is computed.

Algorithm 6.1. (`follow_branch`)

(1) Input: bifurcation point (λ, a), one critical eigenvector $e \in \mathbb{R}^M$ and a stepsize $\Delta\lambda < 0$. The subroutine writes a file with the first part of a bifurcating branch.
(2) Write (λ, a) to output file. Set $t = 0.1$. Set $\lambda_b = \lambda$.
(3) Compute index k so that $|e_k| \geq |e_i|$ for all $i \in \{1, \ldots, M\}$.
(4) Repeat until $\lambda_b - \lambda < \Delta\lambda$, or $t < 0.1/32$ or some maximum number of points have been written to the file.
    (a) Do the pmGNGA with initial guess $(\lambda, a + t\,e)$, fixing coefficient k.
    (b) If Newton's method converges replace (λ, a) by the solution found and write this point to the file, else $t \leftarrow t/2$.

Note that the pmGNGA can follow a branch that bifurcates to the right or the left. Those that bifurcate to the right usually turn over in a saddle-node "bifurcation" that does not offer any difficulty for the pmGNGA. Figures 7 and 8 show several examples of bifurcations.

In the bifurcations with $\mathbb{Z}_3$ and $\mathbb{Z}_6$ symmetry in our problem, the EBL does not hold: The 2-dimensional center eigenspace does not have a one-dimensional subspace with more symmetry. Figure 8 shows one of the few examples bifurcations with $\mathbb{Z}_3$ symmetry that we observed. By good fortune, the branches with symmetry type S_{19} were successfully followed using the same eigenvectors one would choose for a bifurcation with $\mathbb{D}_3$ symmetry. A better method for following bifurcating solutions that are not predicted by the EBL would be to use the pmGNGA with random (normalized) eigenvectors in E repeatedly until it appears that all equivalence classes of solutions have been found.

The branch following code is called recursively by a main Perl script. Initially, the C++ program follows the trivial branch on a given λ range. This results in an output file for the trivial branch and another output file for each bifurcating primary branch. Then the short parts of the primary branches are followed with more calls to the C++ program. Any bifurcating branch results in a new output file, and the Perl script makes another call to the C++ program to continue that branch. The main Perl script's most important job is book keeping. It saves the output files with distinct names, and calls the branch following code to continue each of the new branches. The process stops when all the branches are fully followed within the given λ range.

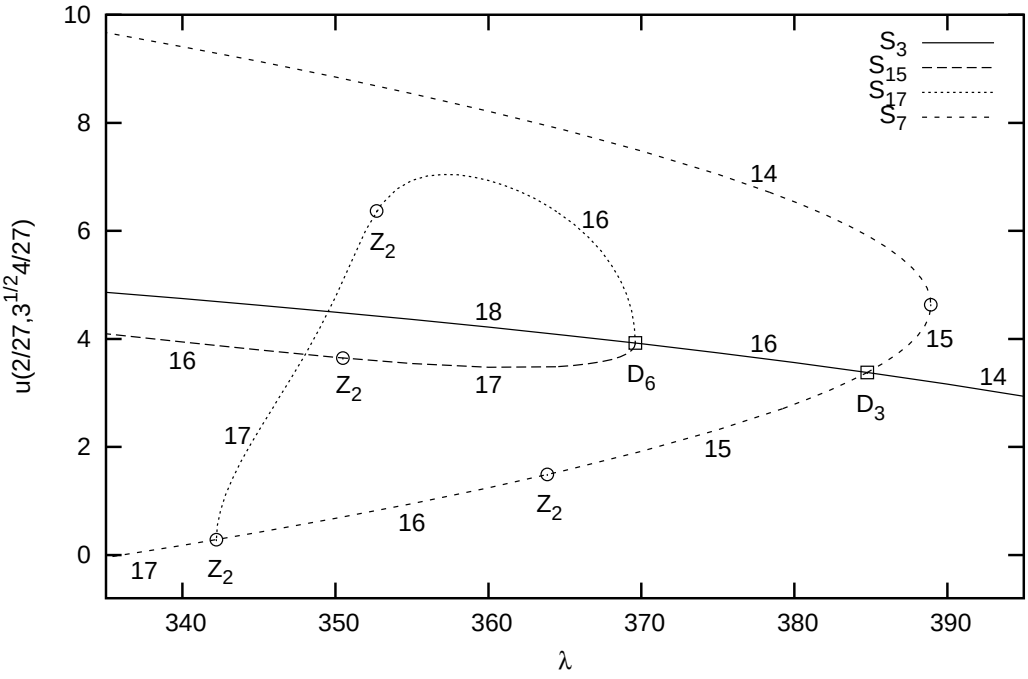

FIGURE 7. A partial bifurcation diagram of the 14-th primary branch showing a $\mathbb{D}_6$, a $\mathbb{D}_3$ and several $\mathbb{Z}_2$ bifurcations. At the $\mathbb{D}_6$ bifurcation, 12 branches in two different group orbits are born. In accordance with Figure 6, only two branches are followed and shown on this bifurcation diagram. An animation showing the followed branch with symmetry type S_{15} is shown in `s3s15.gif`, and an animation of the followed branch with symmetry type S_{17} is in `s3s17s7.gif`. Note that this branch with S_{17} symmetry "dies" at a bifurcation with $\mathbb{Z}_2$ symmetry, showing that we cannot always make a consistent distinction between secondary and tertiary branches. At the $\mathbb{D}_3$ bifurcation, 6 branches in two different group orbits are born. As before, only two branches are followed. An animation showing the "upper" branch with symmetry type S_7, through the bifurcation point and continuing to the "lower" branch with symmetry type S_7 is shown in `s7s3s7.gif`. For clarity, the branches bifurcating from 3 of the $\mathbb{Z}_2$ bifurcations are not shown. The numbers next to a branch indicate the MI of the solution. The MI changes by 2 at a square, and by 1 at a circle.

In this way, a complete bifurcation diagram is produced by a single invocation of the main Perl script. There is no need to guess initial conditions for input to Newton's method, since the trivial solution is known exactly ($a = 0$) and all the other solutions are followed automatically.

The main Perl script calls several other smaller scripts. For example, there is a script which extracts solutions from output files and feeds them to the branch following code as input. Another script creates Gnuplot scripts on the fly to generate bifurcation diagrams. Branch following results in a great number of output files. The organization is an important task. Perl scripts are used to automatically number and store the output files and create human readable reports about them.

7. Numerical Results.

Our goal was to find solutions to (1, 2) at $\lambda = 0$ with all 23 symmetry types. The 24-th primary branch is the first one with symmetry type S_2, so we followed the first 24 primary branches. With level $\ell = 5$ and $M = 300$ modes, which gave our most accurate results, this found solutions with all symmetry types except S_{11} and S_{14}. We then searched the first 100 primary branches, only following solutions with symmetry above S_{11} and S_{14} on the bifurcation digraph (Figure 5.) In this

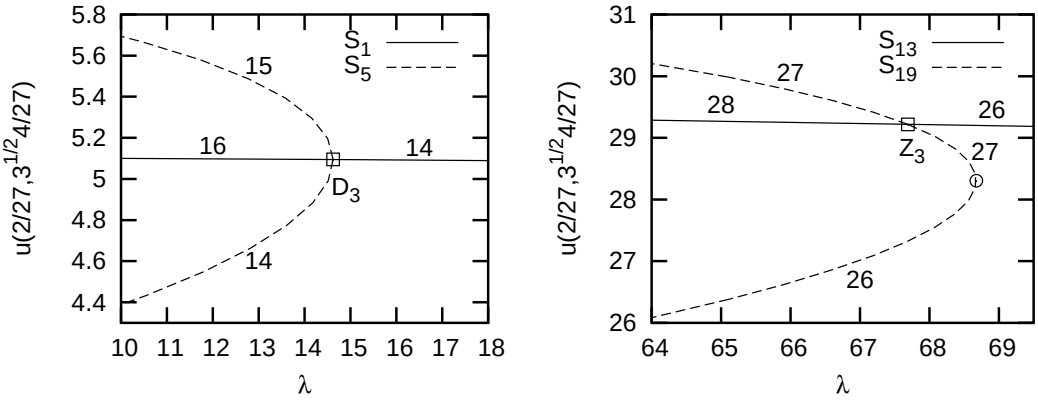

FIGURE 8. The $\mathbb{D}_3$ bifurcation of the 13-th primary branch is on the left. This is the only observed $\mathbb{D}_3$ bifurcation that is not transcritical. An animation of the upper branch with symmetry type S_5, through the bifurcation point and continuing with the lower branch is shown in `s5s1s5.gif`. A $\mathbb{Z}_3$ bifurcation of a daughter of the 24-th primary branch is shown on the right. The branches created at this bifurcation are not described by the EBL. An animation of the branches with symmetry type S_{19} is shown in `s19s13s19.gif`. The bifurcation digraph in Figure 5 indicates that there are possible bifurcations with $\mathbb{Z}_6$ symmetry. We did not observed such a bifurcation with level $\ell = 5$ and $M = 300$ modes.

way we found solutions with all 23 symmetry types. The bifurcation diagrams which lead to these solutions are shown in Figures 9–12. We chose one solution at $\lambda = 0$ with each symmetry type by taking the one descended from the lowest primary branch. These choices are indicated by dots in Figures 9–12, and the corresponding contour diagrams of the solutions are shown in Figures 13 and 14. The contour diagrams use white for $u > 0$ and black for $u < 0$, and gray indicates $u = 0$. Equally spaced contours are drawn along with dots for local extrema. Details about the technique for generating these contour diagrams are found in [20].

At level $\ell = 5$ we have computed 300 eigenfunctions so $M \leq 300$ is possible. At level $\ell = 6$ we computed only 100 eigenfunctions. Due to our limited computational resources, using more than 100 modes on level 6 was not practical. We ran our experiments using a range of modes and levels in order to observe convergence and qualitative stability of the implementation of our algorithm.

As an indication of the convergence, consider the bifurcation diagram in Figure 9. The diagram looks qualitatively the same for any choice of ℓ and M that we used. The position of the bifurcation point creating the S_{10} solution (near $\lambda = 30$) changes slightly, according to this table:

	$\ell = 4$	$\ell = 5$	$\ell = 6$
$M = 100$	35.3931	34.9814	34.9252
$M = 200$	32.1131	32.2964	
$M = 300$		32.0518	

.

The level 5 and 6 approximations with $M = 100$ modes are very close, but increasing the mode number has more of an effect. This indicates that the results with $(\ell, M) = (5, 300)$ are more accurate than those with $(6, 100)$. Figure 15 shows how $u(2/27, 4\sqrt{3}/27)$ varies with mode number and ℓ for the solution with S_{10} symmetry at $\lambda = 0$ shown in Figures 9 and 13. The horizontal segments of the graphs correspond to the addition of modes with zero coefficients for this solution. Based on this and other similar convergence results, we chose to use level 5 with 300 modes in most of our numerical experiments.

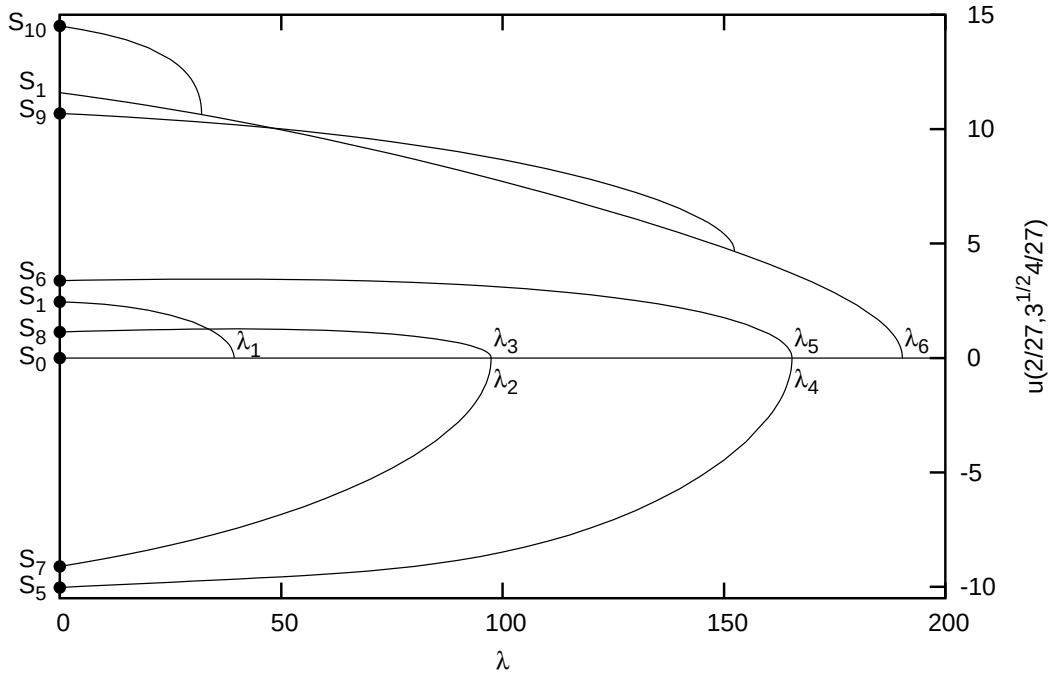

FIGURE 9. The complete bifurcation diagram for the first six primary branches bifurcating from the trivial branch. Primary branch j is labelled by the eigenvalue λ_j at which it bifurcates. The branches born at multiple eigenvalues are labelled so that the j-th primary branch has MI j near the bifurcation. The second branch, with symmetry S_7, contains the CCN solution. The dots at $\lambda = 0$ in Figures 9–12 correspond to solutions depicted in Figures 13 and 14. We used the level 5 grid with 300 modes in creating all bifurcation diagrams. In Figure 15 convergence data for the solution of symmetry type S_{10} at $\lambda = 0$ is provided.

8. Conclusions.

We are currently working on a more general program for recursive branch following in symmetric systems. Our goal is to write a suite of programs that will create the full bifurcation diagram with a single command for any one-parameter gradient system $\nabla J(\lambda, u) = 0$, where $J : \mathbb{R} \times \mathbb{R}^n \to \mathbb{R}$ is $(\Gamma \times \mathbb{Z}_2)$-invariant, Γ is a permutation group acting on $\mathbb{R}^n$, and the nontrivial element of $\mathbb{Z}_2$ acts on $\mathbb{R}^n$ as $-I$. In the current paper, the group $\mathbb{D}_6$ acts as permutations on $G_N \cong \mathbb{R}^N$, the space of functions on a grid.

Starting with any graph, the analog to Equation 1 is the Partial *difference* Equation (PdE) $Lu + f(u) = 0$ [18], where L is the well-known discrete Laplacian on that graph and u is a real-valued function on the vertices. Discretizing a PDE as we have done in this paper leads to a PdE on a graph with a large number of vertices. (The grid points are the vertices of the graph, and the edges of the graph connect nearest neighbor grid points.) Our new branch-following program will be able to compute the bifurcation diagram for the PdE on an arbitrary graph.

The programs we describe in the current paper will work with other superlinear odd f and other regions with hexagonal symmetry. The nonlinearity f needs to be superlinear since our program assumes that the branches eventually "go to the left." Our general program will not have this restriction; the GNGA and pmGNGA will be replaced by a single method of branch following that is able to go through fold points, and has no prejudice about the parameter increasing or decreasing. This new method of branch following has already been successfully implemented in [27]. We hope

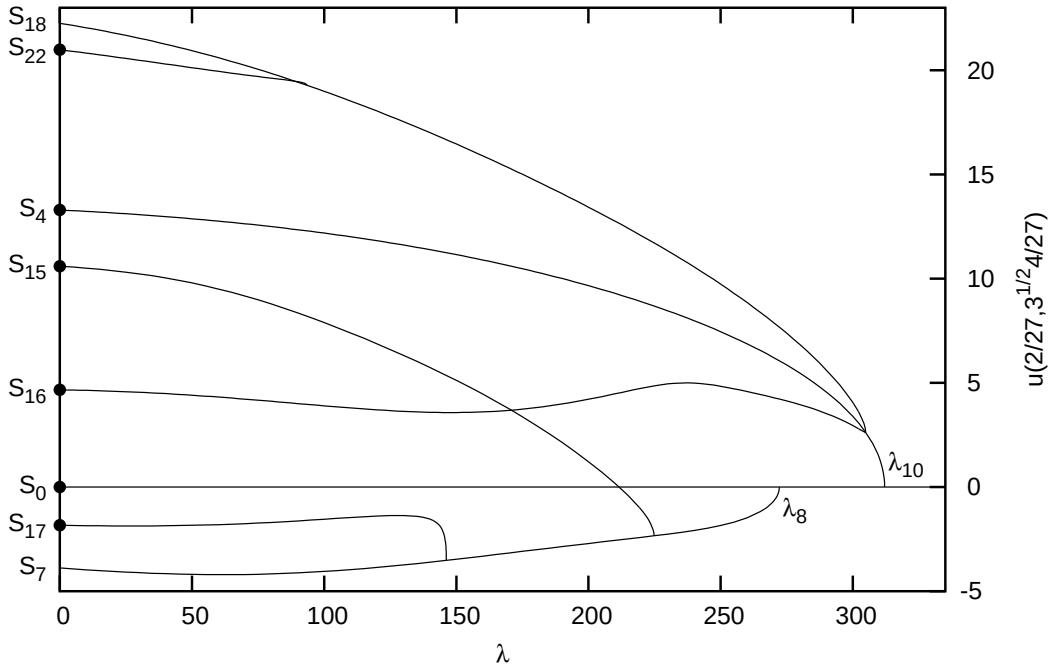

FIGURE 10. A partial bifurcation diagram showing some of the solutions bifurcating from the 8-th and 10-th primary branches. Again, the dots at $\lambda = 0$ indicate solutions shown in Figures 13 and 14. The contour plots as a function of λ are animated for the branches ending with the dots indicating symmetry types S_{15} (`s7s15.gif`), S_{17} (`s7s17.gif`), S_{16} (`s4s16.gif`), and S_{22} (`s4s18s22.gif`).

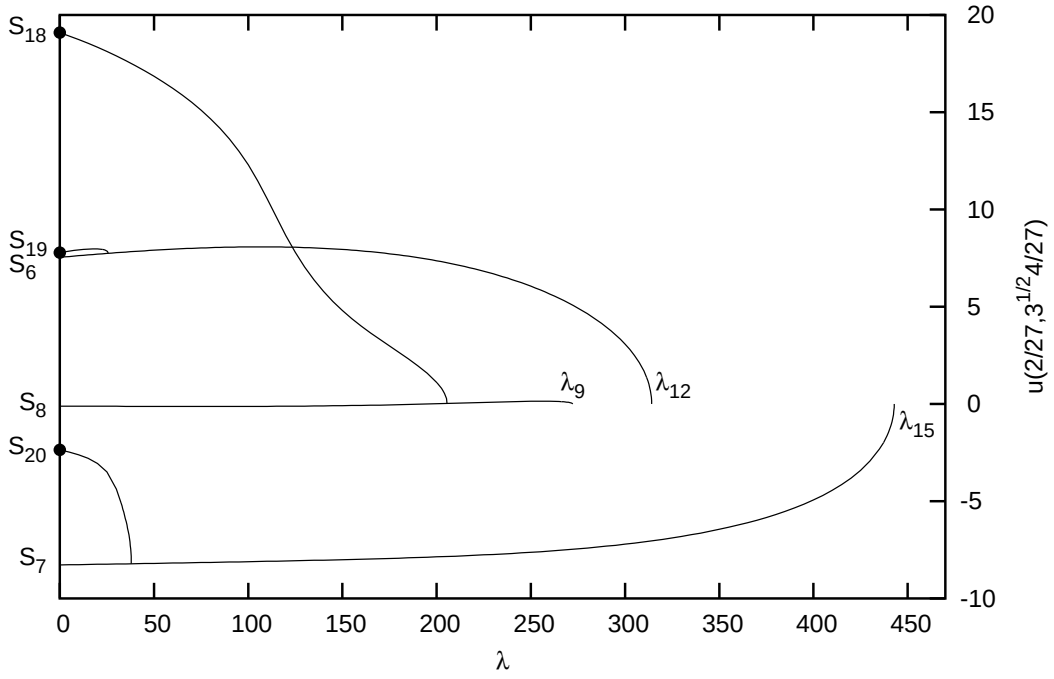

FIGURE 11. A partial bifurcation diagram providing three additional symmetry types. For clarity, the trivial branch is not shown in this and the next figure.

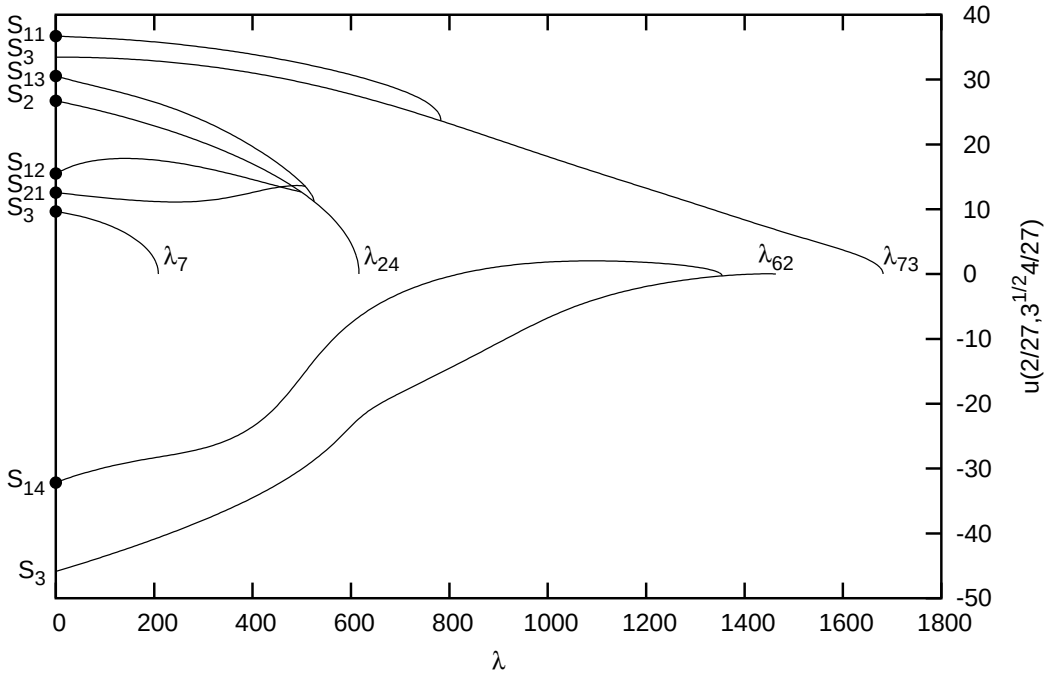

FIGURE 12. A partial bifurcation diagram containing solutions of the seven remaining symmetry types. Primary branch 24 is the first branch with symmetry type S_2. The symmetry types S_{14} and S_{11} were found by searching the first one hundred primary branches, following only those branches which can lead to solutions with the desired symmetry. These two solutions are included for completeness, but their existence for the PDE would have to be confirmed with more modes and a higher level approximation of the eigenfunctions.

to write the new code so that a cluster of computers can be used in parallel, with each computer following a single branch at one time, under the control of a central PERL script.

While our program assumes that is f is odd, it could work for non-odd f with minimal modification. When f is non-odd, only subgroups of $\mathbb{D}_6$ are isotropy subgroups. We would have to check for false identification of isotropy subgroups, but that would happen rarely. The hardest case would be if f_λ is non-odd and $f_\lambda(0) = 0$ (for example $f_\lambda(u) = \lambda u + u^2$ if $u \geq 0$ and $f_\lambda(u) = \lambda u + u^3$ if $u < 0$.) In this case $u = 0$, would be a solution for all values of the parameter λ, and the program described in this paper would think that the symmetry of $u = 0$ is $\mathbb{D}_6 \times \mathbb{Z}_2$ when it is actually $\mathbb{D}_6$. At bifurcations of $u = 0$, the eigenfunctions ψ_j and $-\psi_j$ would spawn two non-conjugate branches whereas the program as it stands would assume that the two branches are conjugate and only follow one of them.

If we used our program without modification for non-odd f_λ that do not satisfy $f_\lambda(0) = 0$ the problem would be that $u = 0$ is not a solution to the PDE. We would have to find at least one solution by trial and error to start the first branch. The simplest procedure would be to find the positive and negative solutions using initial guesses of the form $u = c\psi_1$. These two solutions could then be used as the starting points for two separate runs of our recursive branch following program.

It is valid to ask the question "does the GNGA converge" (as implemented in this current research). While we do not have a complete proof affirming the positive of this conjecture, many references contain relevant theorems. The GNGA is an implementation of Newton's method, which indeed converges under standard assumptions. In [10], one finds the classical fixed point iteration proof that Newton's method in $\mathbb{R}^N$ converges when the initial guess is sufficiently close to a

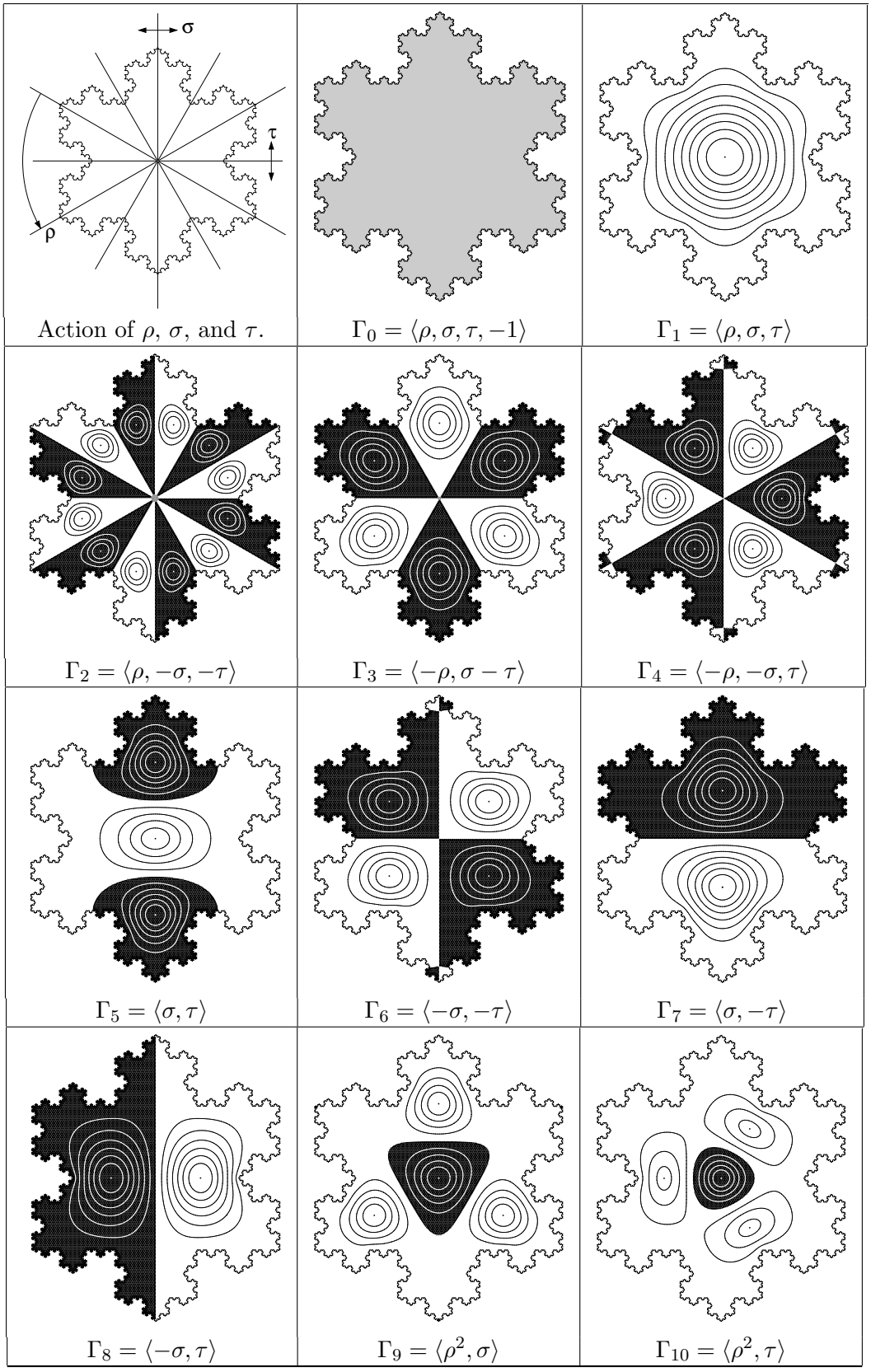

FIGURE 13. The action of the generators of $\mathbb{D}_6$ on the plane, along with contour plots of solutions with symmetry types $S_0, \ldots, S_{10}$ at $\lambda = 0$. Recall that $S_i = [\Gamma_i]$.

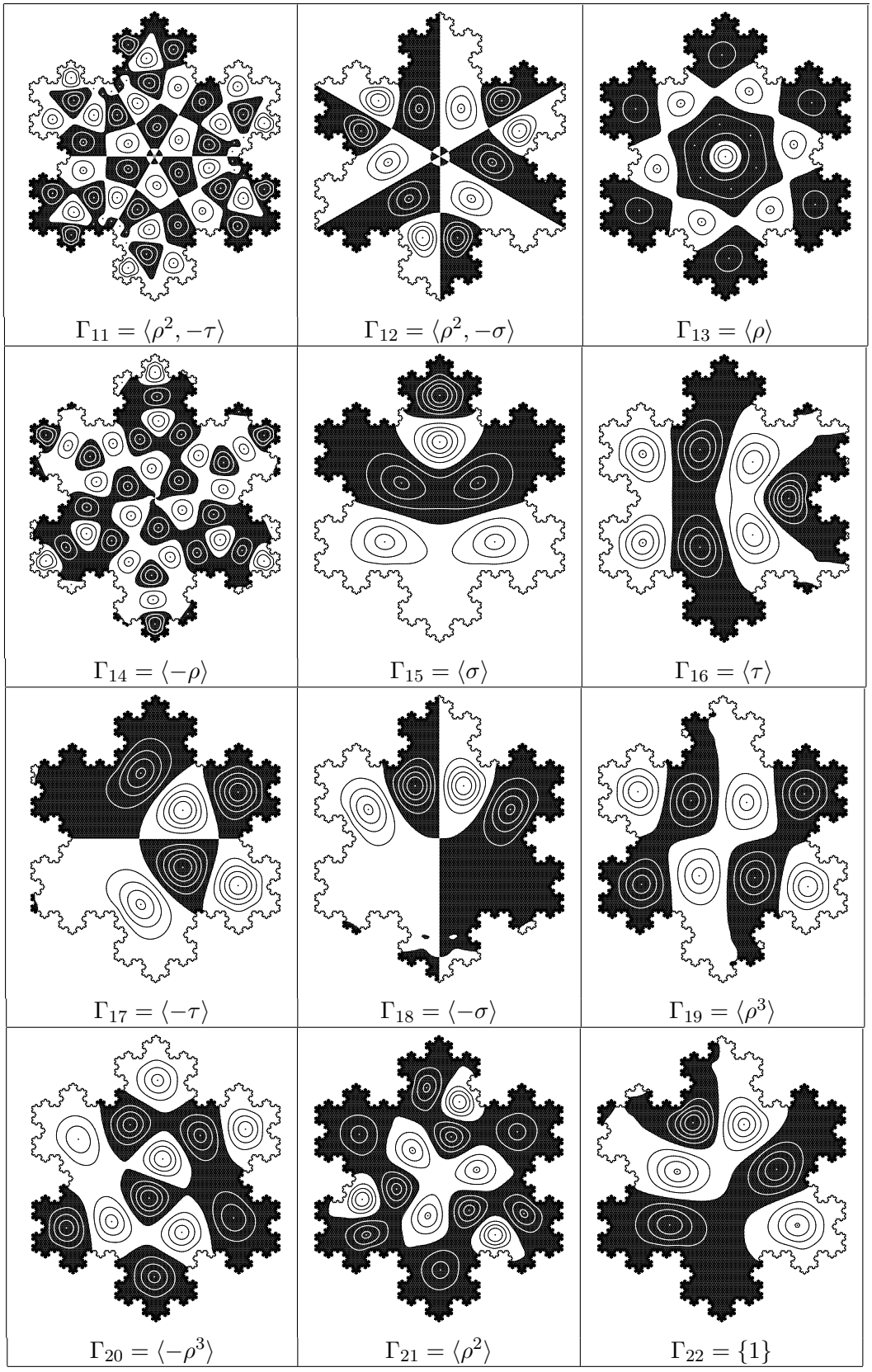

FIGURE 14. Contour plots of solutions with symmetry types $S_{12}, \ldots, S_{22}$ at $\lambda = 0$.

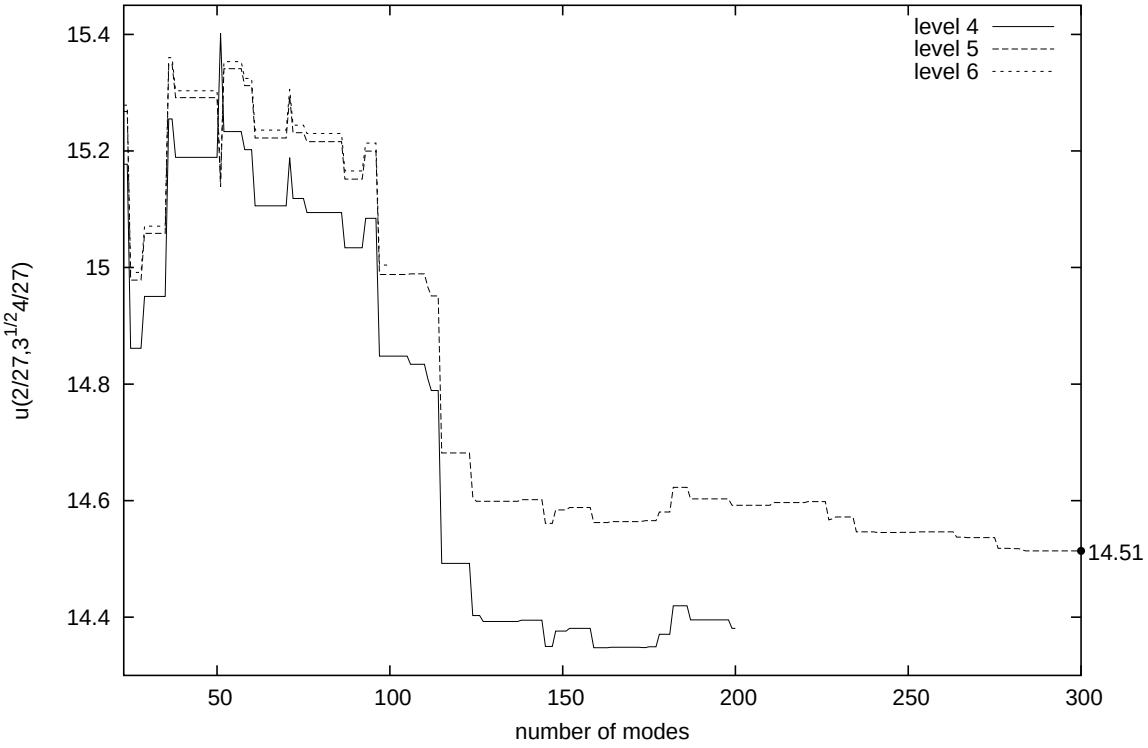

FIGURE 15. A plot of $u(2/27, 4\sqrt{3}/27)$ as a function of the number of modes for the lowest energy solution at $\lambda = 0$ with symmetry type S_{10}. The point at $M = 300$ matches the point labelled with S_{10} in Figure 9. The curves cross near $M = 50$ because ψ_{51} at level $\ell = 4$, and ψ_{52} at levels 5 and 6 approximate the same eigenfunction. Similarly, ψ_{52} at level $\ell = 4$, and ψ_{51} at levels 5 and 6 approximate the same eigenfunction. This unusual labelling happens because the approximate eigenvalues of the two eigenfunctions in questions are ordered differently at $\ell = 4$ and $\ell = 5$, whereas $\lambda_{51} < \lambda_{52}$ by definition.

nondegenerate zero of the object function. This proof applies almost without change to the infinite dimensional case. Also addressed in [10] are algorithms where the object function and/or its derivative are only approximated; this would apply to our implementation due to numerical integration errors, as well as owing to our imperfect knowledge of the eigenfunctions and corresponding eigenvalues. While not discussed exactly in the cited literature, elementary fixed point arguments indicate that the restriction of our object function ∇J to sufficiently large subspaces B_M will still result in convergent iterations. It would be worthwhile to string these type of results together in order to obtain a "best possible" GNGA convergence theorem. The companion monograph [9] gives an easy introduction into some of the details of implementing Newton's method to solve nonlinear problems. Further, in the spirit of [4] and [29], by the invariance of the Newton map, any convergence result should hold in fixed point subspaces corresponding to a given symmetry type. The articles [13, 29] and others by those authors discuss the convergence of algorithms similar to the GNGA, at times also considering symmetry restrictions. Finally, the well known book [1] contains relevant convergence results for Newton and approximate Newton iterative fixed point algorithms.

In summary, we have written a suite of programs that automatically computes the bifurcation diagram of the PDE (1, 2). The program follows all of the solution branches which are connected to the trivial branch by a sequence of symmetry-breaking bifurcations. A thorough understanding of

the possible symmetry-breaking bifurcations is required for this task. We introduced the bifurcation digraph, which summarizes the results of the necessary symmetry calculations. For the group $\mathbb{D}_6 \times \mathbb{Z}_2$, these calculations were done by hand and verified by the GAP computer program [5, 14]. In the future, we plan to implement automated branch following in systems where the symmetry group is so complicated that GAP is necessary.

References

[1] Berger, M. S. *Nonlinearity and functional analysis. Lectures on nonlinear problems in mathematical analysis*, Pure and Applied Mathematics. Academic Press [Harcourt Brace Jovanovich, Publishers], New York-London, 1977. xix+417 pp.

[2] Castro, A., J. Cossio and J. M. Neuberger, *Sign-Changing Solutions for a Superlinear Dirichlet Problem*, Rocky Mnt. J. Math **27**, no. 4, pp. 1041–1053 (1997).

[3] Castro, A., P. Drabek and J. M. Neuberger, *Sign-Changing Solutions for a Superlinear Dirichlet Problem, II*, Proceedings of the Fifth Mississippi State Conference on Differential Equations and Computational Simulations, EJDE **10** (2003).

[4] Costa, D., Z. Ding and J. M. Neuberger, *A Numerical Investigation of Sign-Changing Solutions to Superlinear Elliptic Equations on Symmetric Domains*, J. Comput. Appl. Math. **131**, no. 1-2, pp. 299–319 (2001).

[5] GAP Group, *GAP – Groups, Algorithms, and Programming,* 2002, `http://www.gap-system.org`.

[6] Golubitsky, M., I. Stewart and D. G. Schaefer, *Singularities and Groups in Bifurcation Theory, Volume 2*. Applied Mathematical Sciences **69** Springer-Verlag, New York, 1988. xvi+533 pp.

[7] Golubitsky, M. and I. Stewart *The Symmetry Perspective: from Equilibrium to Chaos in Phase Space and Physical Space*, Progress in Mathematics **200**, Birkhäuser Verlag, Basel, 2002. xviii+325pp.

[8] Hineman, J. and J. M. Neuberger, *Numerical Solutions to Semilinear Elliptic BVP on Bunimovich Stadia*, to appear, Comm. Nonlin. Sci. Num. Sim. (2005).

[9] Kelley, C. T. *Solving Nonlinear Equations with Newton's Method. Fundamentals of Algorithms*, Society for Industrial and Applied Mathematics (SIAM), Philadelphia, PA, 2003. xiv+104 pp.

[10] Kelley, C. T. *Iterative Methods for Optimization. Frontiers in Applied Mathematics*, **18** Society for Industrial and Applied Mathematics (SIAM), Philadelphia, PA, 1999. xvi+180 pp.

[11] Lapidus, M. L., J. W. Neuberger, R. L. Renka, and C. A. Griffith, *Snowflake Harmonics and Computer Graphics: Numerical Computation of Spectra on Fractal Drums*, International Journal Bifurcation and Chaos **6**, no. 7, pp. 1185–1210 (1996).

[12] Lehoucq, R. B., D. C. Sorensen, and C. Yang *ARPACK users' guide: Solution of large-scale eigenvalue problems with implicitly restarted Arnoldi methods. Software, Environments, and Tools.* Society for Industrial and Applied Mathematics (SIAM), Philadelphia, PA, 1998. xvi+142 pp.

[13] Li, Y. and Zhou, J. *Convergence Results of a Local Minimax Method for Finding Multiple Critical Points*, SIAM J. Sci. Comput. **24**, no. 3, pp. 865–885 (electronic), (2002).

[14] Matthews, P. C., *Automated Symmetry-Breaking Calculations*, LMS J. Computational Math. **7**, pp. 101–119, (2004).

[15] Neuberger, J. W., *Sobolev Gradients and Differential Equations*, Lecture Notes in Mathematics, **1670**. Springer-Verlag, Berlin, 1997. viii+150 pp.

[16] Neuberger, J. M., *A Numerical Method for Finding Sign-Changing Solutions of Superlinear Dirichlet Problems*, Nonlinear World **4**, no. 1, pp. 73–83, (1997).

[17] Neuberger, J. M., *GNGA: Recent Progress and Open Problems for Semilinear Elliptic PDE*, Variational methods: open problems, recent progress, and numerical algorithms, Contemp. Math., **357**, Amer. Math. Soc., Providence, RI, pp. 201–237, (2004).

[18] Neuberger, J. M., *Nonlinear Elliptic Partial Difference Equations on Graphs*, to appear, J. Experimental Math, (2005).

[19] Neuberger, J. M. and J. W. Swift *Newton's Method and Morse Index for Semilinear Elliptic PDEs* International Journal Bifurcation and Chaos **11**, no. 3, pp. 801–820, (2001).

[20] Neuberger, J. M., N. Sieben and J. W. Swift, *Computing Eigenfunctions on the Koch Snowflake: A New Grid and Symmetry*, to appear, J. Comp. and App. Math, (2005).

[21] Neuberger, J. M., J. W. Swift, and T. J. Thompson, *Newton's Method for Solutions of a Ginzburg-Landau Equation on a Thin Disk*, in preparation, (2005).

[22] Rabinowitz, P., *Minimax Methods in Critical Point Theory with Applications to Differential Equations*, CBMS Regional Conference Series in Mathematics, **65**. Published for the Conference Board of the Mathematical Sciences, Washington, DC; by the American Mathematical Society, Providence, RI, 1986. viii+100 pp.

[23] Scott, W. R., *Group theory*, Prentice-Hall, Inc., Englewood Cliffs, N.J. 1964. xi+479 pp.

[24] Smoller, J. and A. G. Wasserman, *Symmetry-Breaking for Positive Solutions of Semilinear Elliptic Equations*, Archives of Rational Mechanics Analysis **95**, pp. 217–225 (1986).

[25] Sternberg, S., *Group Theory and Physics*, Cambridge University Press, Cambridge, 1994. xiv+429 pp.
[26] Thomas, A. D. and G. V. Wood, *Group Tables*, Shiva Mathematics Series, **2**. Shiva Publishing Ltd., Nantwich; distributed by Birkhuser Boston, Inc., Cambridge, Mass., 1980. 174 pp.
[27] Thompson, T. J., *Estimating Solutions for the Ginzburg-Landau Superconductivity Model in Thin Disks*, M. S. Thesis, Northern Arizona University, (2005).
[28] Tinkham, M., *Group Theory and Quantum Mechanics*, McGraw-Hill Book Co., New York-Toronto, Ont.-London, 1964. xii+340 pp.
[29] Wang, Z-Q and J. Zhou, *A Local Minimax-Newton Method for Finding Multiple Saddle Points with Symmetries*, SIAM J. Numer. Anal. **42**, no. 4, pp. 1745–1759 (electronic), (2004).
[30] Zhou, J. and Z.-Q. Wang, *An Efficient and Stable Method for Computing Saddle Points with Symmetries*, preprint, to appear in SIAM J. Num. Anal., (2005).

E-mail address: John.Neuberger@nau.edu, Nandor.Sieben@nau.edu, Jim.Swift@nau.edu

Department of Mathematics and Statistics, Northern Arizona University PO Box 5717, Flagstaff, AZ 86011-5717, USA